POLITECNICO DI MILANO

School of Industrial and Information Engineering

Master of Science in Materials Engineering and Nanotechnology

Department of Chemistry, Materials and Chemical Engineering "G.Natta"

EFFECTS OF PROCESSING ON ULTIMATE STRENGTH OF

COMPOSITE LAMINATES

Supervisor: Roberto FRASSINE

Co-supervisor: Luca MEZZO

Master Thesis of:

Mauro RAVAIOLI

ID: 783552

Academic Year: 2013 – 2014

INDEX

LIST OF FIGURES

LIST OF TABLES

ABSTRACT

Nowadays composite materials in marine sector are increasingly employed in high performance applications. The manufacturing process of composites parts is crucial. Voids, fibres misalignment during lamination and tools drops during processing can affect drastically the final mechanical properties of a component. The aim of this work is to study the consequences in compressive and interlaminar shear strength (ILSS) of these factors in carbon/epoxy unidirectional laminates. Plates have been produced following both a standard manufacturing and different lamination processes, namely varying the cure pressure and the frequency at which the debulk operation was carried out. With ultrasonic scans and acid digestions has been evaluated the effect of the lamination on the voids, remarking the influence of debulk in no-pressure cure cycle. Compressive tests with various set up were not able to reproduce reliable results, whereas in ILSS have been tested successfully also samples with fibre misalignment from 2° up to 10° degrees, and a group previously subjected to drop-weight impact tests with energy ranging from 0,5 to 34J. As anticipated by ultrasonic testing, debulk operation was found affecting more in no pressure cure cycle that the ones at high pressure. A linear trend has been found for the strength at varying the degree of misalignment and the post-impact testing has allowed to identify a threshold in impact energy beyond which strength rapidly decrease.

Keywords: composite materials; carbon fibres; ILSS; fibres misalignment; low velocity impact; BVID.

ESTRATTO IN ITALIANO

I materiali compositi nel settore nautico oggigiorno sono sempre più impiegati per applicazioni dove sono richieste alte prestazioni. Il processo di fabbricazione di manufatti con questi materiali è cruciale. Vuoti, disallineamento delle fibre in fase di laminazione e la caduta di utensili durante la lavorazione possono influire drasticamente sulle proprietà meccaniche finali. Lo scopo di questo lavoro è quello di studiare le conseguenze di questi fattori sulla resistenza alla compressione e al taglio interlaminare (ILSS) di laminati unidirezionali in fibra di carbonio / resina epossidica. Il materiale è stato prodotto seguendo sia un processo standard sia considerando delle variazioni ad esso, ossia variando la pressione di cura e la frequenza alla quale l'operazione debulk veniva effettuata. Con scansioni agli ultrasuoni e digestioni acide è stato valutato l'effetto della laminazione sui vuoti, sottolineando l'influenza del debulk nei cicli di cura senza pressione. Dalle successive caratterizzazioni a compressione, effettuate con diverse tipologie di set up, non è stato possibile ottenere risultati affidabili. Si sono invece ottenuti risultati attendibili da prove ILSS, effettuate anche su campioni tagliati con disallineamento delle fibre da 2° fino a 10° gradi e su un gruppo precedentemente sottoposto a prove di impatto a basse velocità, con energie di impatto che spaziavano da 0,5 a 34J. Come anticipato dai test ad ultrasuoni, l'operazione di debulk si è rivelata un parametro importante nei cicli di cura senza pressione, mentre in quelli ad alta pressione non ha determinato variazioni dello stesso ordine di grandezza. Un comportamento lineare è stato osservato nella resistenza al variare del disallineamento delle fibre mentre la caratterizzazione dopo impatto ha permesso di identificare una soglia di energia oltre la quale la resistenza cala bruscamente.

Parole chiave: materiali compositi; fibre di carbonio; ILSS; disallineamento delle fibre; impatti a bassa velocità; BVID.

PREFACE

The purpose of this work, carried out in collaboration with Future Fibres, is the evaluation of the decrease in strength in unidirectional composite laminates at various manufacturing and processing conditions. In particular, it has been of interest to compare the effects of different laminations, lay up misalignment and impact in both compressive and interlaminar shear strength.

The materials required for the characterisation have been supplied by Future fibres and have been produce directly at the company headquarter in Valencia during Erasmus experience, in order to respect as much as possible the real condition of manufacturing. It has been produce material following a standard procedure, in order to determine the reference properties from a consolidated process. Different laminations have been taken into account to evaluate the relative influence on the generation of voids and thus, the effect on mechanical properties. Two cure cycles have been considered. The first at 5 bar of pressure, the second one only in vacuum bag, and It has been focused the attention on the incidence of the debulk operation in both processes.

Before testing the materials produced, the quality has been checked by ultrasonic inspection at the laboratories of non-destructive techniques (NDT) of Alenia-Aermacchi. Through the ultrasonic scan in transmission and pulse echo it has been possible to evaluate the effective influence of the lamination processes on the plates produced, observing different porosity levels. These Porosity levels have been controlled also by acid digestion.

At Politecnico di Milano, the plates produced have been cut in specimens that have been subsequently tested. In a preliminary phase, several attempts were carried out to characterise the material in compression. No one of the different set-up considered were able to give reliable results with the machine at disposition.

10

On the contrary, the interlaminar shear strength (ILSS) tests have provided reproducible and reliable values. Three groups of samples, one for each batch considered in the present work, were machined from plates produced with a standard process and tested. After a statistical analysis to verify the homogeneity of the results, the values obtained were used as a reference for comparison with subsequent tests. For any typology of manufacturing processes considered a group of samples were tested.

From the material produced with standard lamination, have been obtained and tested also samples with various degrees of misalignment from the fibres direction, searching a trend in the decrease of strength.

A large group of samples was finally subjected to drop-weight testing with increasing impact energy level, remarking detrimental effects on strength already at low impact energies.

1   INTRODUCTION

1.1   COMPOSITE MATERIALS IN MARINE SECTOR

A Composite material consists in the combination at a macroscopic level of two or more constituents that are not soluble in each other. One constituent is called the reinforcement and may be in the form of fibres, particles or flakes. The continuous phase in which the reinforcement is embedded in, is called the matrix.
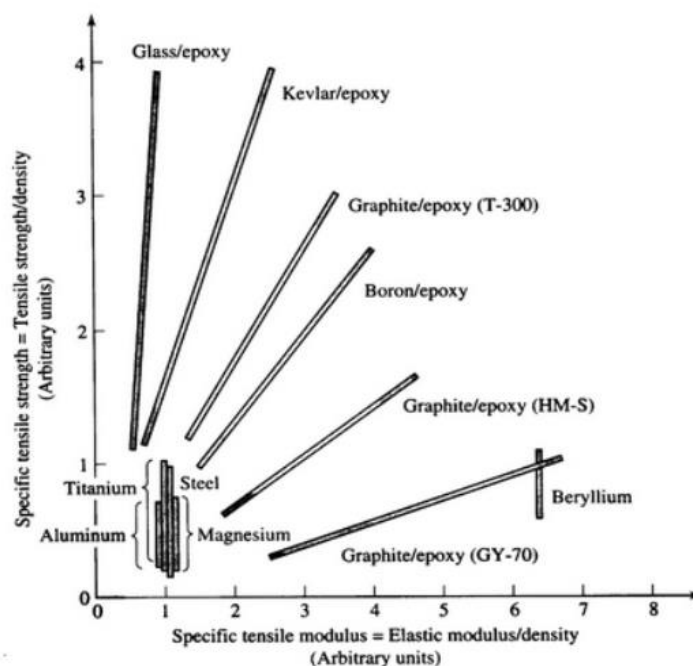
Figure 1.1: Specific tensile strength against specific tensile modulus. Comparison between common used metals

This particular interaction in which each material preserve its identity, leads to a combination of properties that cannot be achieved with either of the constituent acting alone. A particular class of composites, in which strong, stiff and long fibre are combined with a matrix of plastic material, thermoset or thermoplastic resins, is called fibre reinforced plastic (FRP). Today's research has made available composite materials with more strength, lighter weight and increased design flexibility. Characteristics that have allowed composites to take the place usually reserved for steel.

Their high specific properties allow to save weight maintaining unaffected the characteristics of safety and reliability of a particular designed structural component (Figure 1.1).

Specific properties of composite materials are widely exploited in marine sector, especially in yacht sailing. A perfect balance and distribution of weights is important to preserve the symmetry of forces acting on each part of a vessel. Every kilogram of weight saved in the upper part of the ship, can be matched by a kilo added to the bulb keel, so improving the yacht's ballast ratio and hence gaining upwind sailing ability [1, 2]. Masts, booms, spreaders, spars but also rigging systems are some of the components where fibres reinforced plastics have successfully replaced traditional materials. As a drawback, manufacturing processes are becoming a crucial element dealing with composite manufacts. Defects already introduced during manufacturing, such as voids or delamination could compromise the design requirements. It is essential to establish an acceptable level of defects in the design. A too conservative criterion would lead to oversized components or discard those that may still provide acceptable performance, all resulting in increasing costs of production. On the other side, if defects were underestimated, catastrophic failure could occur. A Criteria for defects acceptability, established through extensive experimental characterization of their effects on mechanical properties, must be adopted.

1.1.1 MATRIX

The matrix must fulfil various task in a composite system. First they hold the structural reinforce along the direction designed, in order to bear correctly the loads. Second, they act as a medium for transmission and distribution to the fibres of the tensions applied at the composite. Third, preserve fibres from the superficial wear because of the interaction with the surrounding environment.

Marine environment is very aggressive; continue exposure to high humidity or direct contact with water leads to its absorption by the majority of resins. This, combined with high temperature working condition, induces stiffness reduction due to plasticization effects and also weakens the interfacial binds between fibres and matrix [3].

Epoxy resins are currently the most used for application in water environment. They are much less prone to water ingress and insensible to humidity than any other resin system. The elevate ability to bind the reinforce, the good mechanical properties and the resistance to chemical agents and corrosion, are all features that makes epoxy the most common resin used when high performance is required. Their versatility is the result of the presence of epoxy rings, that make possible the processing with a great variety of molecular groups and thus with the different types of reinforce.
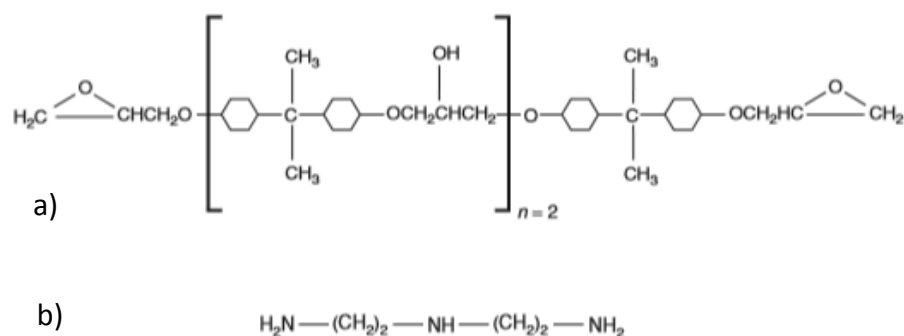
Figure 1.2: (a) Molecule of diglycidyl ether of bisphenol-A (DGEBA). (b) Molecule of diethylene triamine (DETA), typical curing agent.

14

The most common prepolimer used as a starting material is the diglycidyl ether of bisphenol-A (DGEBA) (Figure 1.2.(a)). It contains two epoxide groups, one at each end of the molecule and it is obtained by the synthesis of bisphenol A with an excess of epichlorohydrin.

(a)

(b)

(c)
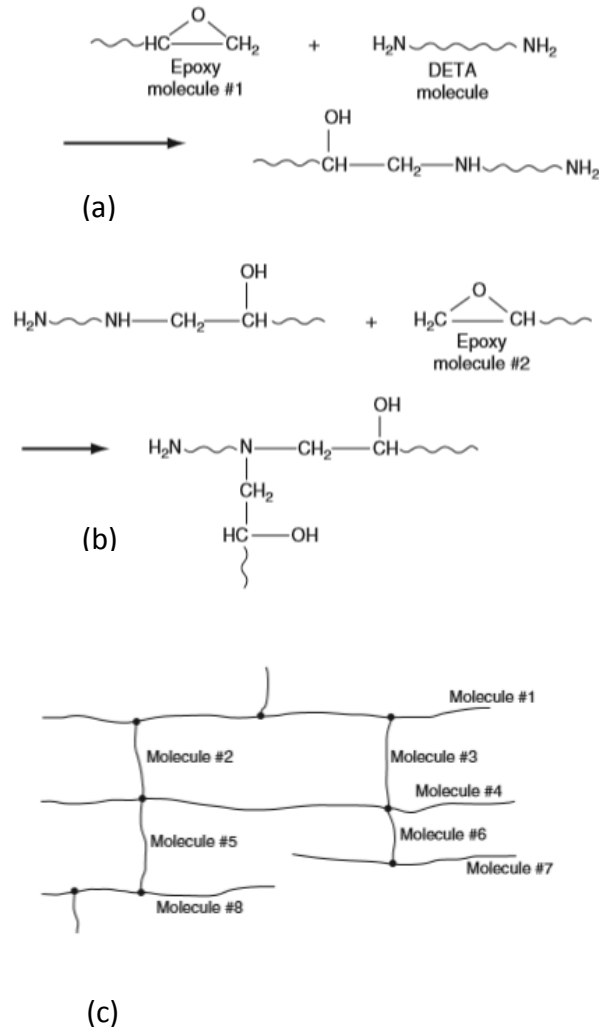
Figure 1.3: Cross-linking reaction of an epoxy resin. (a) Reaction of one epoxide ring with one DETA molecule. (b) Formation of the cross-links (c)the final three-dimensional network structure.

DGEBA is a low molecular weight liquid resin, which needs to be cured with the addition of a crosslinking agent, such as diethylene triamine (DETA) (Figure 1.2.(b)), and to be heated to reach the final solid state. During the polymerization the hydrogen atoms in the amine groups of a DETA molecule react with the epoxide groups of DGEBA.

As the reaction continues, more and more cross-links between each molecules of DGEBA are formed, and the typical three-dimensional network structure is generated (Figure 1.3.(c)).

The properties of a cured epoxy resin depend principally on the cross-link density. The nature and the quantity of curing agent added to the starting prepolymer determine the further curing cycle, the morphology of the chemical structure and so, all the mechanical properties of the resin [4].

1.1.2 FIBRES

Fibres are used in unidirectional composites by aligning a large number of them in a thin plate or shell called lamina, layer or ply. The fibres possess better properties than the relative bulk material due to the preferential orientation of the molecules along the fibre direction and the reduced number of defects present. The most common fibres used in composites are glass, carbon, organic (Kevlar), boron, silicon carbide and alumina. In the present work, prepregs with unidirectional carbon fibres are used.
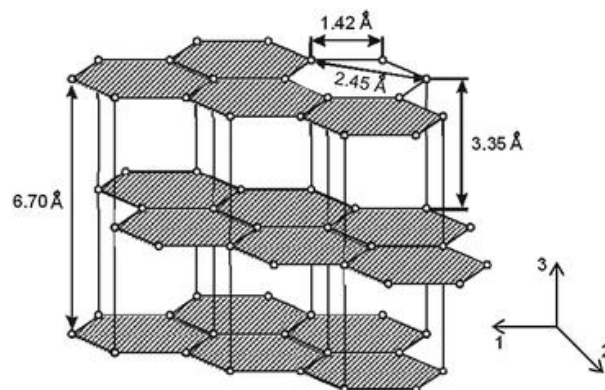
Figure 1.4 : Crystalline structure of graphite.

Carbon fibres are commonly used as reinforce for their excellent specific mechanical properties. Thanks to their high strength, stiffness and lightness, they play an important role in advance composites. The most stable crystalline structure for carbon in standard condition is the graphite. In graphite, carbon atoms are ordered in parallel sheets of planar hexagonal cells as shown in Figure 1.4.

Atoms of the same plane are bounded each other through strong covalent bonds, whereas weak interaction forces of Van Der Waals bind the different sheets. The important consequence of the crystalline structure is the anisotropy of carbon fibres that is exploited to obtain specific high properties along preferential direction. The fibres are obtained through pyrolysis of various organic precursors such as rayon or pitch, but nowadays over 90% of the total carbon fibres manufacturing use polyacrylonitrile (PAN) as a precursor (Figure 1.5).
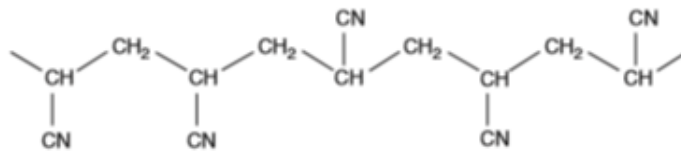
Figure 1.5: A macromolecule of polyacrylonitrile.

In the process that use PAN as starting material, the polyarilonitrile fibres are first stretched five to ten times their length to align the polymer chain in the filament direction and then are subjected to three heating processes. In the first, called stabilization, the fibres passed through a furnace between 200°C and 300°C in air to be partially oxidize, and in this phase cyanide groups join together to form a rigid ladder structure (Figure 1.6).
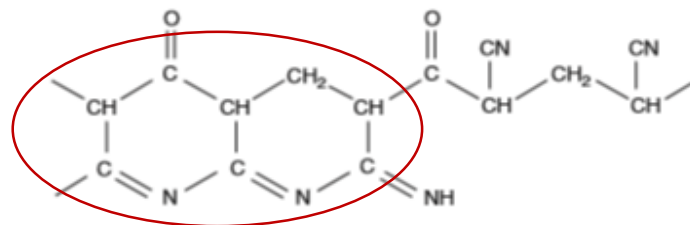
Figure 1.6: Oxidized PAN, highlighted the formation of the ladder structure

In the second process, called carbonization, the filaments are pyrolysed in an inert atmosphere between 1000°C and 1500°C to remove oxygen and nitrogen atoms. At this stage carbon atoms are already arranged in aromatic rings patterns that lay in parallel planes, but a further heat treatment is needed to have a perfect ordered structure. The last step is called graphitization and fibres are heated above 2500°C to obtain a structure more similar to the true graphite (Figure 1.4).
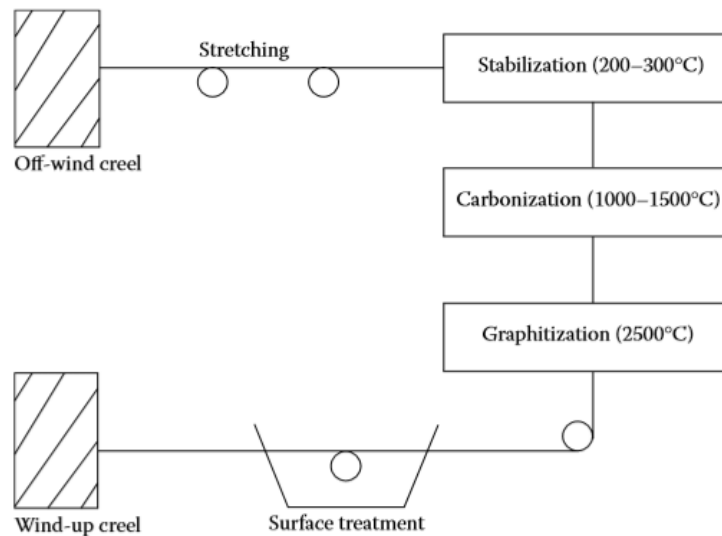
Figure 1.7: All the stages of the standard manufacturing process of carbon fibres.

The fibres modulus is tuned by the degree of crystallinity and the degree of orientation of the fibres. Increasing maximum pyrolysis temperature and applying tension during the last two stage of the process is possible to obtain fibres with an elasticity modulus of over 500 GPa. At the end of the three-step heat treatment process, the fibres surface is treated to preserve them from premature rupture during further machining operation, and to obtain a suitable substrate for adhesion to the matrix. In fact It is important to have a good interfacial adhesion for a correct transfer of load between matrix and fibres [5].

18

1.1.3 PREPREGS

The material used in the present work is a unidirectional epoxy based prepreg system. Prepregs consist in pre-impregnated fibres with resin that has underwent a partial reticulation.

A row of uniformly spaced fibres passes through a resin bath containing catalysed epoxy resin dissolved in a solvent. Fibres preimpregnated with liquid resin are then passed through a chamber in which heat is applied to advance the curing reaction to an intermediate stage. At this stadium, the resin is partially cross-linked and is characterised by a stickiness (*tack*) which allows the positioning during the lamination process. The sheets of preinpregnated fibres are then backed up with a release film to avoid sticking together and then wound around a take-up roll. The backup material is separated from the prepreg sheet just before it is placed in the mould to manufacture the composite part. The Prepregs rolls are conserved at a temperature of -18°C to slow down the kinetics of the crosslinking reaction, in order to avoid complete consolidation before the lamination process.
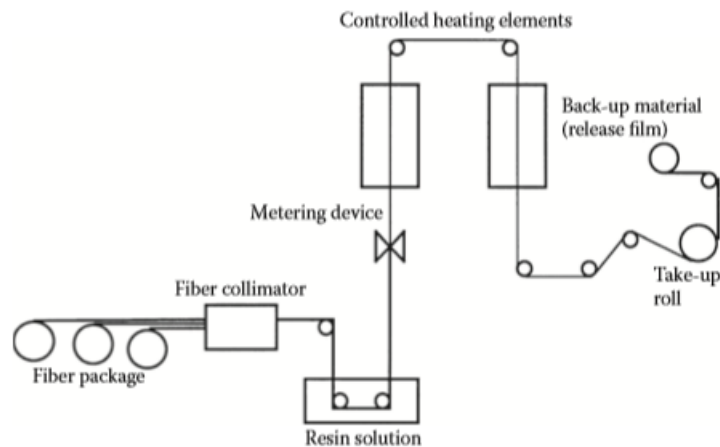
Figure 1.8: Stages of a common manufacturing process of prepregs.

Lamination process consists in two passages: first, the stack up of a sequence of sheets and then the consolidation of the manufact in autoclave with temperature and pressure specific for the resin.

After being stacked up, the pile of sheets are covered with a peel-ply to leave an imprint or pattern on the surface to enhance adhesive bonding for further machining. A breather–bleeder combination is added to help distribute the vacuum and to channel the volatiles with the excess of resin to vacuum port. The composite manufact is then sealed in a vacuum bag and consolidated in autoclave. The vacuum helps to withdraw excess of volatile compounds, such as residual solvents, trapped air, or low molecular weight components of the resin, and avoids the formation of voids during the cross-linking.

The autoclave is a pressure vessel that contain compressed gas able to reach high pressure during the cure cycle. In the first stage of the curing, called dwelling, the temperature is raised to decrease the resin viscosity until it reaches the minimum value. Then temperature is kept constant in this crucial stage to let the resin flow, to promote the compenetration of the laminas and thus to reduce the void content in the cured laminate. Augmented pressure increases the compaction, promoting consolidation of the plies and the extraction of excess resin. At the end of the temperature dwelling, a further increase of temperature is required to start the crosslinking reaction. Molecular weight and viscosity rapidly increase until a unique network of macromolecule is reached [6].

1.2 LONGITUDINAL COMPRESSIVE STRENGHT OF COMPOSITE

The compressive strength is the value of uniaxial compressive stress reached when a material fails completely under the action of a compressive load. In the case of composites the failure mechanism on compression depends strongly on the nature of these materials. In FRP the matrix phase has the important function of provide lateral support and stability for fibres under compressive loading. However, the mismatch between the relative low modulus of the matrix compared to the high one of the fibres, causes the onset of localized instability, such as fibres microbuckling, which ends in a failure of the total component.

In unidirectional laminates under the effect of compressive longitudinal loads, several competitive mechanisms of failure arise [7].

- Elastic microbuckling: it's a shear buckling instability and the matrix deforms in simple shear (Figure 1.9.(a)).
- Plastic microbuckling: shear instability that occurs at sufficiently large strains for the matrix to deform in a non linear manner (Figure 1.9.(b)).
- Fibres crushing: failure occurs at fibre level of scale due to a shear instability such as buckling within the fibre. It is often associated with the fact that the fibres themselves are microcomposites comprising wavy fibres embedded in a soft matrix (Figure 1.9.(c)).
- Splitting: matrix forms crack parallel to the main axial fibres direction. It is associated with a low toughness of the matrix (Figure 1.9.(d)).
- Buckle delamination: this occurs by the buckling of a surface layer from a sub-surface debond. Post impact compressive strength is often a concern in the use of composites, as the impact event leads to a large debond. Subsequent compressive loading can induce a buckle delamination growth. Buckle delamination is associated with a low matrix toughness and the presence of a large subsurface flaw (Figure 1.9.(e)).
- Shear band formation: Matrix yield and fracture occur in a band, oriented at about 45° respect to the loading axis (Figure 1.9.(f)).
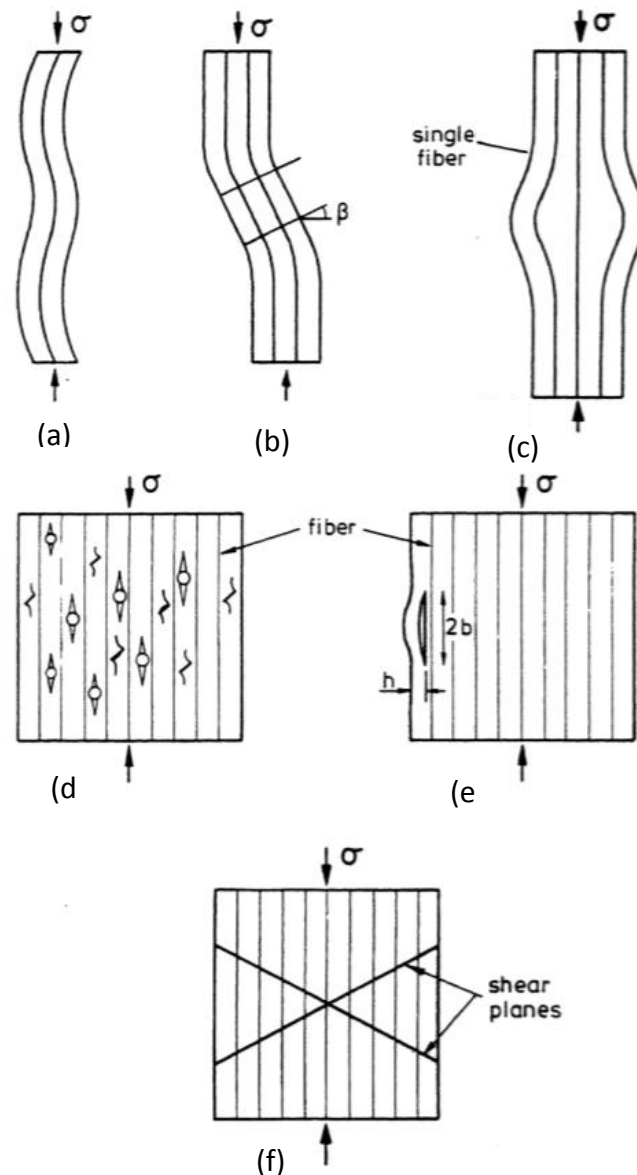
Figure 1.9: Principal failure mechanism of composite materials. (a) Elastic microbuckling. (b) Plastic microbuckling. (c) Fibres crushing. (d) Splitting of the matrix. (e) Buckle delamination of surface layer. (f)Shear band formation.

In carbon/epoxy unidirectional laminates it is found that the dominant mechanism of failure is the plastic microbuckling in the form of fibres kinking [8](Figure 1.10). Under compressive loads, failure onset is controlled by fibres misalignment combined with plastic shear deformation in the matrix. The waviness of the fibres along their directions is due to several factors. Among them, the fact that as soon as they are produced, fibres are wound into spools, which induce natural curvature in the fibres.

When stretched in to a flat mould, they tend to curl slightly. Moreover, thermoset polymers tend to shrink during the cure, whereas fibres don't, thus fibres must accommodate the strain generated by the matrix in the form of waviness. It is assumed that the fibres within a band of infinite length and finite width ω suffer an initial uniform misalignment $\bar{\varphi}$. In addition, the band of misalignments is tilted from the fibres direction by an angle β. The first model proposed by Argon considered a kinking within a β=0 band for a rigid perfectly plastic composite with longitudinal shear strength τ_{12}. When the shear stress generated in the band kink due to compressive load becomes equal to the shear strength, instability is generated and this can bring to rupture.

$$\sigma_{US} = \frac{\tau_{12}}{\bar{\varphi}}$$

<div align="right">1</div>

The previous formulation was extended by Budiansky to an elastic-perfectly plastic composite with in plane shear modulus G and in plane ultimate shear strain $\gamma_{12}=\tau_{12}/G$:

$$\sigma_{US} = \frac{G}{1 - \dfrac{\bar{\varphi}}{\gamma_{12}}}$$

<div align="right">2</div>
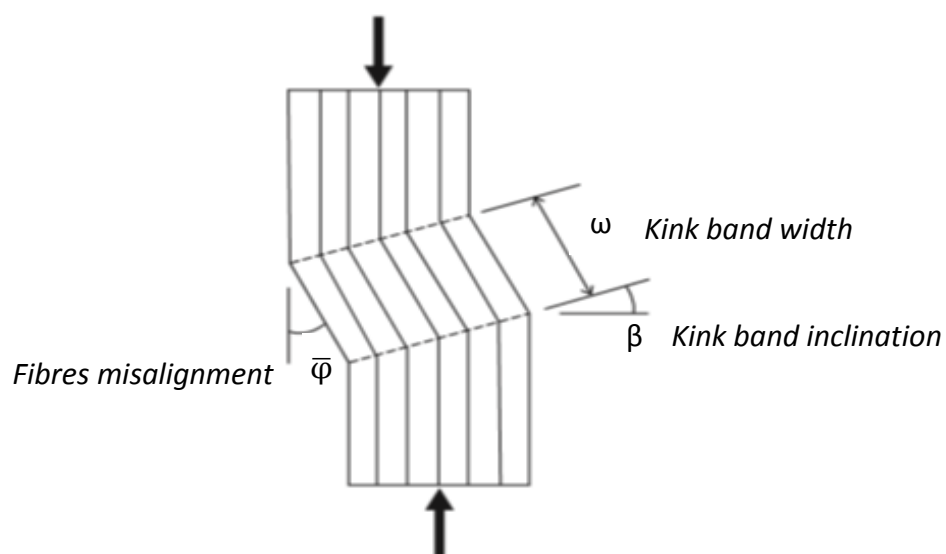
Figure 1.10: Fibres kinking mechanism.

1.3   INTERLAMINAR BEHAVIOUR OF COMPOSITES

1.3.1 SHEAR IN CLASSICAL BEAM THEORY

Transverse loads generate both bending moments $M(x)$ and shear forces $V(x)$ along the beam. The bending moments cause bending normal stresses σ to arise through the depth of the beam, and the shear forces cause transverse shear-stress distribution through the beam cross section as shown in the Figure 1.11 .
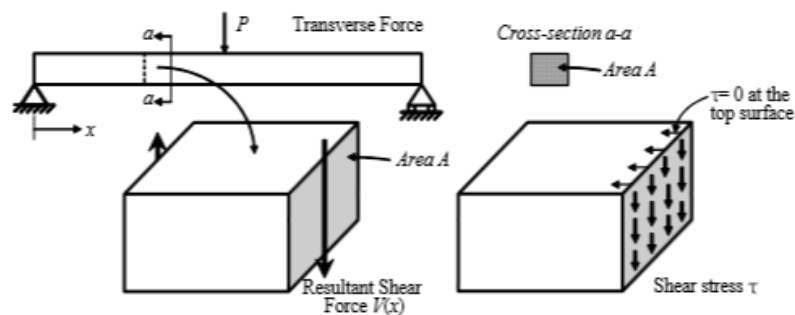
Figure 1.11: Beam with transverse shear force showing the transverse shear stress developed by it

Cross sections are assumed to remain plane and perpendicular to the longitudinal axis of the beam after deformation. This assumption is violated when the beam is subjected to both bending and shear, but if we assume small displacement, the cross-sectional warping described above remains small enough and can be neglected .
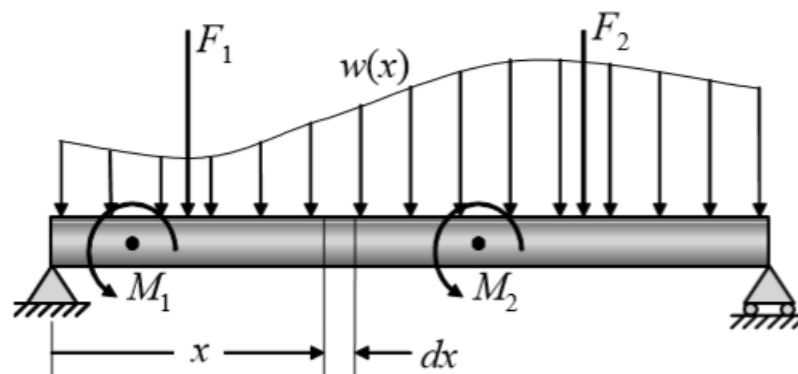
Figure 1.12: Simply supported beam with examples of applied loads

When considering the free body diagram of the element *dx,* with bending moment stress distribution only as in Figure 1.13, no transverse forces are taken into account if only horizontal equilibrium is considered.
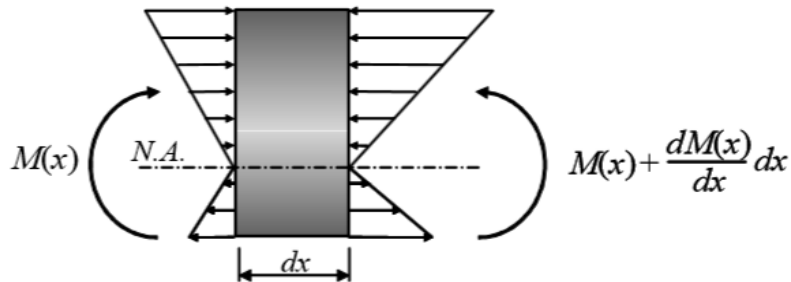
Figure 1.13: Element of the beam with length dx and normal stresses arisen due to the bending moment

Summing the forces horizontally on this infinitesimal element, the stresses due to the bending moments only form a couple, therefore the force resultant is equal to zero horizontally. Considering a distance y above the neutral axis (N.A.) up to the top of the element, a shear stress τ_{xy} must be present in order to be in equilibrium, as shown in Figure 1.14.
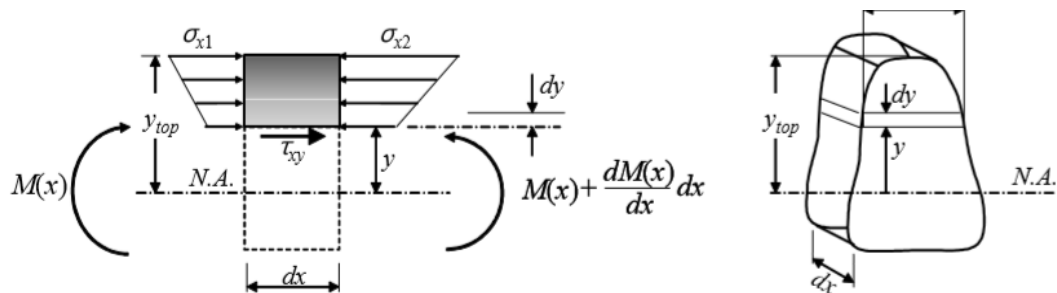
Figure 1.14: Segment of length dx cut at distance y from the N.A., with equilibrating shear stress τ_{xy}.

The width of the section at a distance y from the neutral axis is set to be a function of y called *t(y).* Applying the horizontal equilibrium equation, gives:

$$\sum F_x = 0 = \int_{y}^{y_{top}} \sigma_{x1} t(y) dy - \int_{y}^{y_{top}} \sigma_{x2} t(y) dy + \tau_{xy} t(y) dx = 0$$

3

Substituting for the magnitude of the stresses the relation derived for pure bend in Euler–Bernoulli theory

$$\sigma_x = \frac{M(x)y}{I}$$

<div align="right">4</div>

gives:

$$\int_y^{y_{top}} \frac{M(x)y}{I} t(y)dy - \int_y^{y_{top}} \frac{(M(x) + dM(x))y}{I} t(y)dy + \tau_{xy} t(y)dx = 0$$

<div align="right">5</div>

Simplifying and dividing by dx and $t(y)$ gives:

$$\tau_{xy} = \frac{dM(x)y}{dx} \frac{1}{It(y)} \int_y^{y_{top}} yt(y)\, dy$$

<div align="right">6</div>

But since

$$V(x) = \frac{dM(x)}{dx}$$

<div align="right">7</div>

then, the shear stress distribution is given by:

$$\tau_{xy} = \frac{V(x)}{It(y)} \int_y^{y_{top}} yt(y)\, dy = \frac{V(x)Q(y)}{It(y)} = \frac{VQ}{It}$$

<div align="right">8</div>

Where $V(x)$ is the shear force carried by the section found from the shear force diagram, I is the second moment of area, $t(y)$ is the sectional width at the distance y from the neutral axis and $Q(y) = \int_y^{y_{top}} yt(y)dy = \bar{y}'A'$. A' is the top (or bottom)

portion of the member's cross-sectional area, defined from the section where $t(y)$ is measured, and $\bar{y}'$ is the distance to the centroid of A', measured from the neutral axis.

1.3.2 SHEAR IN A RECTANGULAR SECTION BEAM

Considered a beam with a rectangular cross-section of width b and height h as indicated in Figure 1.15, the distribution of the shear stress throughout the cross section due to a shear force V can be determined by computing the shear stress at an arbitrary height y from the neutral axis.

$$Q = \bar{y}'A' = \left(y + \frac{1}{2}\left(\frac{h}{2} - y\right)\right) \times \left(\left(\frac{h}{2} - y\right)b\right) = \frac{1}{2}\left(\frac{h^2}{4} - y^2\right)b$$

9
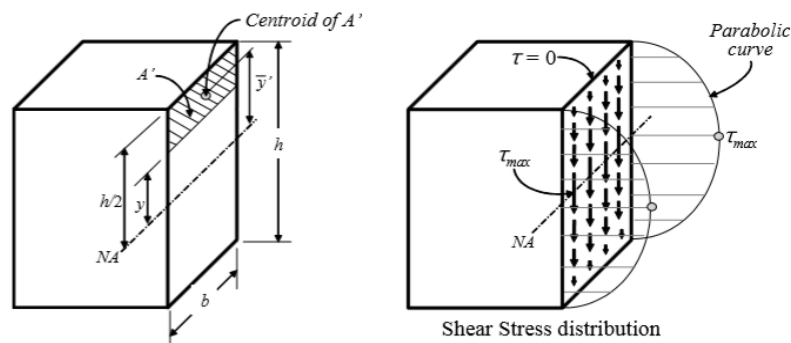
Figure 1.15: Distribution of shear stress in a rectangular beam

The second moment of inertia for the entire area is simply:

$$I = \frac{bh^3}{12}$$

10

With $t = b$, applying the shear formula the subsequent equation is obtained:

$$\tau_{xy} = \frac{VQ}{It} = \frac{V \times \frac{1}{2}\left(\frac{h^2}{4} - y^2\right)b}{\frac{bh^3}{12} \times b} = \frac{6V}{bh^3}\left(\frac{h^2}{4} - y^2\right)$$

11

The result indicates that the shear stress distribution over the cross section is parabolic. The shear force intensity varies from zero at the top and bottom, where $y = \pm h/2$, to a maximum value at the neutral axis at $y = 0$. In the specific case of a simply supported beam, loaded in the middle with a concentrated load P, vertical constraint force of magnitude of $P/2$ arise at the hinge and at the roller as shown in Figure 1.16 :
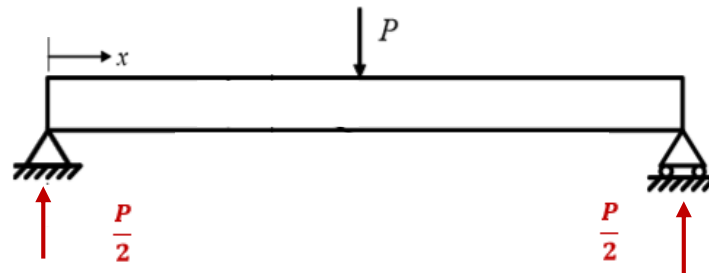
Figure 1.16: Simply supported beam with load at the centre.

The relative shear force diagram is the following:

$$V(x) = \begin{cases} \dfrac{P}{2} & for\ 0 \le x \le \dfrac{L}{2} \\ -\dfrac{P}{2} & for\ \dfrac{L}{2} < x \le L \end{cases}$$
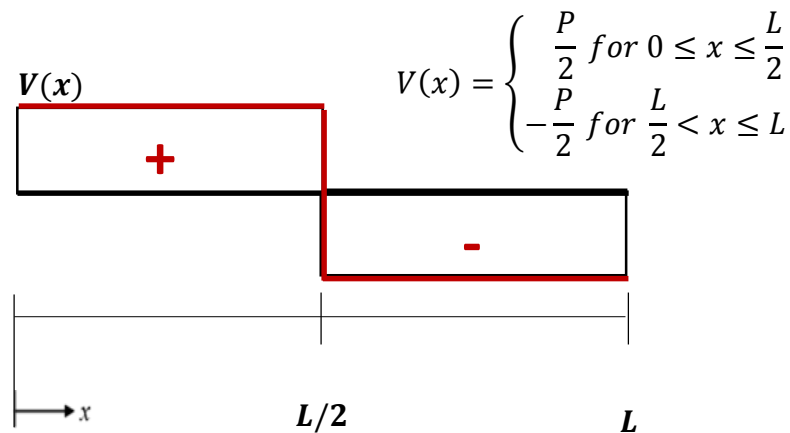
Figure 1.17 : Diagram of the shear force in a simply supported beam load at the centre.

The maximum shear stress, that occurs at the neutral axis, is obtained substituting V(x) in the equation 11:

$$\tau_{max} = \frac{3}{4}\frac{P}{bh}$$

1.3.3 INTERLAMINAR SHEAR STRENGTH OF COMPOSITES

Interlaminar stress are defined as the stress acting in the interface of two adjacent plies in composite laminates. They may cause delamination failure, the most critical failure mode in laminated composite materials. Thus, a good knowledge of such stresses can prevent catastrophic event in the lifecycle of a composite component. These stresses cause relative deformations between adjacent plies. If the corresponding strength values, that are constant for a particular composite material, are exceeded by these stresses, failure along the interface takes places. During the design of a component, there are two approaches to characterize the delamination resistance: the strength-of-materials approach and the linear elastic fracture mechanics approach (LEFM). Though is an aspect of fundamental importance in design, LEFM approach is out of the purpose of the present work thus attention will be focused on the strength-of-materials approach.
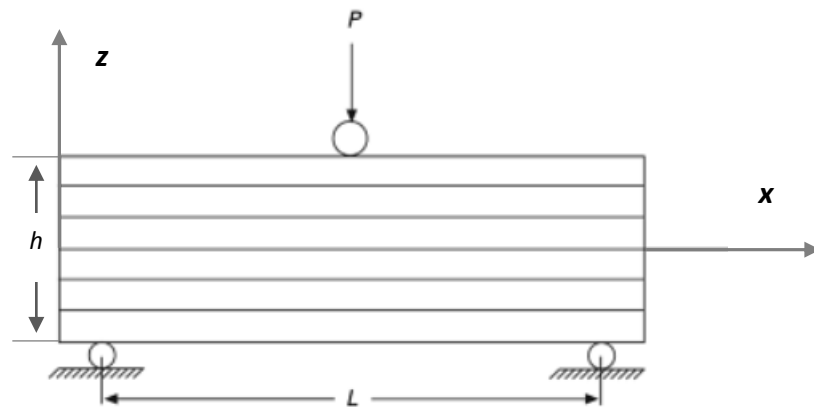
Figure 1.18: Example of a short beam shear test load and supports.

In the strength-of-materials approach, the interlaminar shear strength (ILSS) is used as the controlling factor for the initiation of delamination. Thus, the determination of the ILSS through appropriate test is of primary importance. The requirement for a correct test is that the initiation of failure in the specimens is induced by only transverse shear mode, but even today, there is no method available for the exact determination of this strength property. It is only possible to determine an approximate value of the interlaminar shear strength, called apparent interlamninar shear strength, by using various test methods such as Short beam shear (*SBS*) test.

This typology provides a known state of relatively uniform stresses and strains in the specimen section, while minimizes the stress concentration in the load introduction section. Unwanted failure modes are prevented by suitable values of geometrical parameters for the test specimen. As seen in the previous section, during three-point bend, shear stress arises and are maximum along the neutral axis of a sample, equation 12, but also flexural stress arise with magnitude

$$\sigma = \frac{3P}{2bh}\left(\frac{L}{h}\right)$$

<div align="right">13</div>

at the top and the bottom of the specimen, being L equal to the distance between the lower supports [4](Figure 1.18).

The shear stress acts in the direction transverse to the beam axis and is significant in the case of relatively short beams. The maximum normal stress in the beam decreases with decreasing the ratio L/h whereas the maximum shear stress at the neutral axis is not affected. For sufficient small L/h (ISO 14130[9] recommends $L/h = 5$) the maximum shear stress in the beam will reach the ILSS of the material even though the maximum normal stress remain sufficiently low.

It may be noted that although all the above mentioned precautions are taken both tensile and compressive flexural failure may take place at the outer plies of the laminated beam, before shear failure at the mid plane takes place. The test specimen could fail by fibres rupture, microbuckling, interlaminar shear cracking or a combination of fracture modes. A check of the failure modes on the specimen is required at the end of each test to discard incorrect values of strength.

1.4 EFFECT OF PROCESSING ON COMPOSITES

The main issue in composites cured in autoclave process is the presence of voids and is an unavoidable fact. Voids are caused by air bubbles and volatiles entrapped in the liquid resin. Solvents used for resin viscosity control, moisture, and chemical contaminants in the resin, may remain dissolved in the resin mix and volatilize during elevated temperature curing. In addition, air is also entrapped between various layers during the lamination process. To avoid the formation of air during this stage, the operation of debulk is required to help the adhesion between plies and as a preventive measure to remove possible entrapped air in the interface between the sheets. The debulk operation consist in seal the top of the partial laminate component with a vacuum bag and the consequent application of vacuum for at least 2minutes up to 30 and is normally carried out every 2-5 plies.
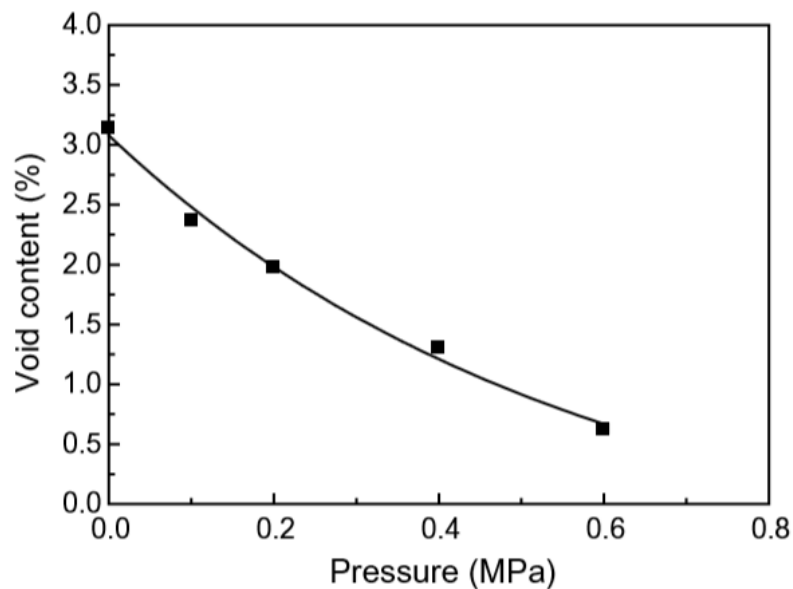
Figure 1.19: Relation between pressure applied during the cure cycle and void content for a graphite/carbon composite

Cure cycles parameters, such as temperature and pressure, have been found to play an important role in the influence of void content in composite laminates(Figure 1.19)[10]. The temperature is usually scheduled recommended by the manufacturers and any modification could alter significantly the structural performance and thus should be avoided. For this reason, the cure cycle pressure is usually considered as

the main process parameter to be optimized. If chosen the properly the amount of pressure and the correct moment of applying, the entrapped air, the water vapour and the excessive resin will be squeezed out from the laminates, and the laminates with low porosity and high performance will be achieved. It is well known that for a graphite/epoxy composite, a matrix dominated failure mechanism such ILSS is strongly effected by void content, more than the flexural strength or tensile strength (Figure 1.20) [10, 11].
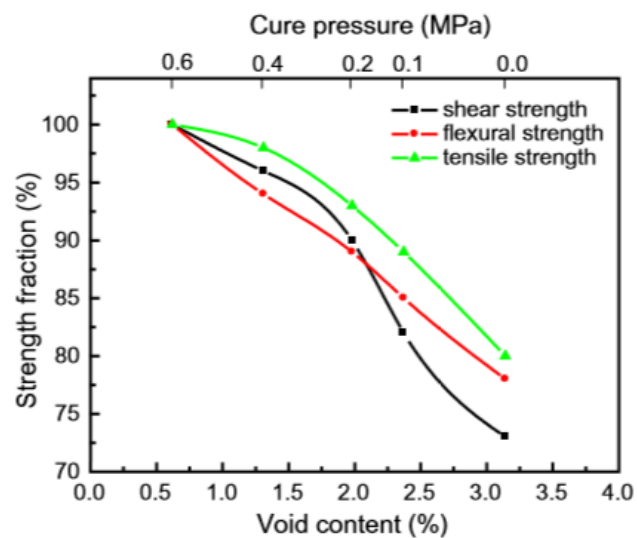
Figure 1.20: Relationship between strength and void contents on a carbon graphite composite

Voids have detrimental effects on the strength of composites but an excessively high acceptance level of design performance requirements is not always a successful strategy. An extremely low presence of voids implies unnecessary high cost of processing when a tolerance design can lead to important cost reduction. Each component is designed for a specific application, thus, establishing the acceptable level of voids for a given working condition is a critical issue.

1.5 IMPACT BEHAVIOUR OF COMPOSITES

Impact damage is generally not considered to be a threat in metal structures, because, owing to the ductile nature of the material, a large amount of energy may be absorbed. In contrast, composites can fail in a wide variety of modes and can contain barely visible impact damage (BVID) which nevertheless severely reduces the structural integrity of the component[12].
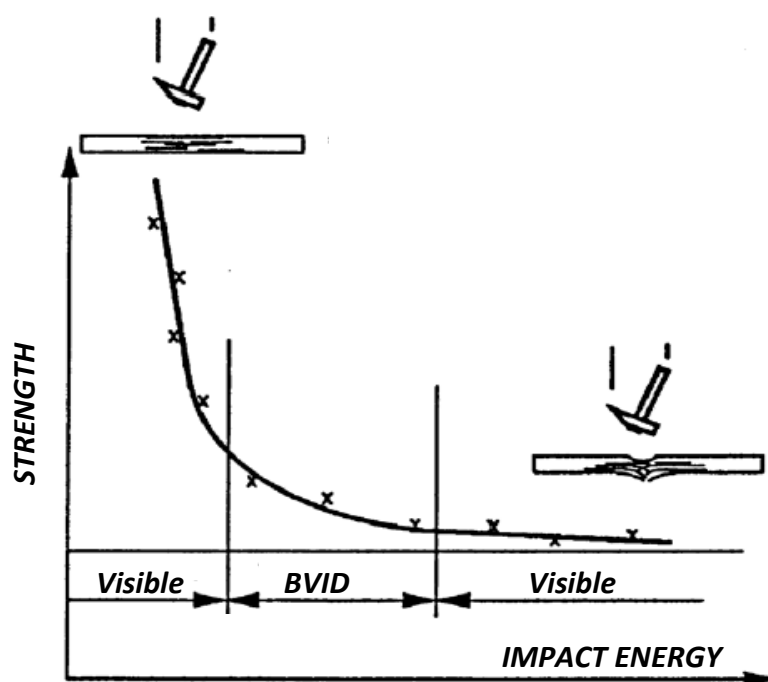
Figure 1.21: Typical trend in reduction of the strength with increasing impact energy

Composites based on epoxy resins are brittle and so can only absorb energy in elastic deformation and through damage mechanisms, and not via plastic deformation. The main issue with composite is that a generic impact produces a damage that reduces severely the strength of a component, even before this could be detected by a normal visible inspection. This implies the need of a periodic monitoring with NDT, such as ultrasonic, and the necessity of prompt evaluation of the damage extend.

The term damage resistance refers to the amount of impact damage that is induced in a composite system. Clearly, the vast majority of impacts on a composite plate will

be in the transverse direction, but, due to the lack of through-thickness reinforcement, transverse damage resistance is particularly poor. Interlaminar stresses-shear and tension are often the stresses that cause the first failure[13, 14]. Generally, impacts are categorized into low, high and, sometimes, also hyper velocity.

High velocity impacts are characterised by localized damage. The response of the material is dominated by the stress wave propagation and the structure does not have time to absorb energy elastically. As a contrary, in low velocity impacts, the contact duration is long enough to let the dynamic response of the material dissipate elastically the energy. Although doesn't exist a unique definition, neither a clear transition for the two categories, it is found in literature that the stress wave doesn't play a significant role in the stress distribution for impact velocity up to 10 m/s .

Usually the first damage that can occur during an impact is in the form of matrix cracking. Cracks are usually oriented in planes parallel to the fibres direction and are caused by properties mismatch between fibres and matrix. There are two typologies of matrix crack. Shear cracks occur in the upper layers and the middle layer, under the edges of the stricker. They are inclined at an angle of approximately 45° and are formed by the very high shear stress through the material. Bending cracks generally occur in the bottom of the laminate[13]. They are found in vertical shape and are caused by high tensile bending stresses.
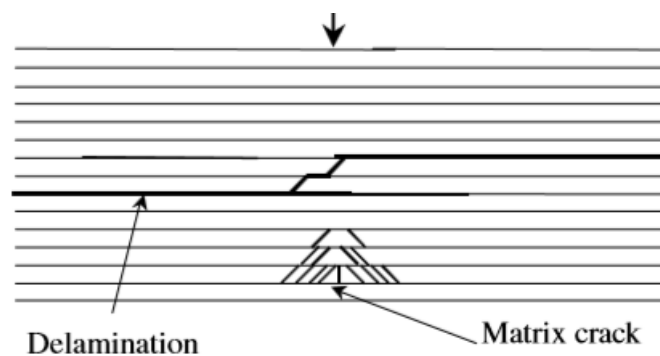
Figure 1.22: Type of damage occurring in impacted composite materials.

Delamination is the result of bending stiffness mismatch between plies, generally due to different fibres orientation (Figure 1.23). The greater is the mismatch, the greater delamination area will be. Transverse impact can cause delamination only if a threshold energy has been reached and it has been observed that it can only occur in the presence of a matrix crack. More precisely delaminations are the result of a mode to fracture process due to very high out-of-plane normal stresses, caused by the presence of the matrix cracks and interlaminar shear stresses along the interface[15].
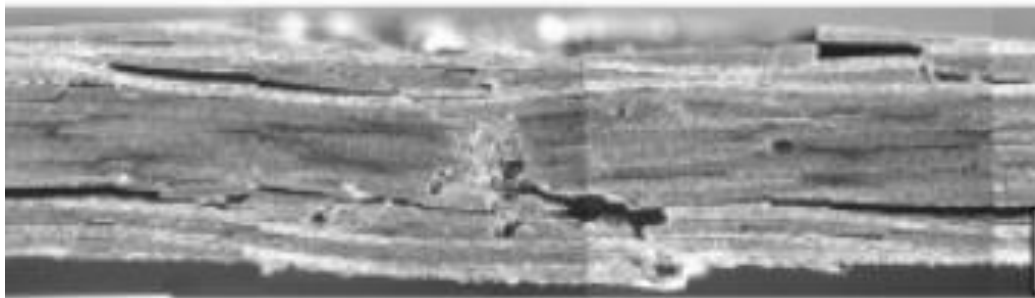
Figure 1.23: Transversal section of an impacted composite plate with high impact energy. Clearly visible the delamination

1.6 STATISTICAL ANALYSIS WITH COMPOSITES

When compared to metallic materials, the base material properties for fibres reinforced composite materials exhibit a high degree of variability. This variability is due to many factors, including, but not limited to, raw material and prepreg manufacture, material handling, part fabrication techniques, ply-stacking sequence, environmental conditions and testing techniques. In some cases, the variation in the defects associated with these factors is the apparent cause. The variability, which is directly related to the test procedures, has been minimized over the years through research and standardization. Nevertheless, the cost of composite testing is relatively high. This, combined with additional testing due to the orthotropic nature of composite materials, has led to smaller data sets for a particular property than those produced for metallic materials. This necessitates the usage of advanced statistical techniques for determining reasonable design allowables for composites. Guidelines are available for statistical analysis when a property of a manufact, such as strength, has to be determined from samples belonging to different batches and groups.

The military handbook of composite materials [16] suggests a one-tailed ANOVA(analysis of variance) test to verify the homogeneity of variance between the results of the groups. This test is based on the assumption that the total variance can be decomposed in the sum of two contributes. The variation *within* the batches and the variation *between* the batches. ANOVA test required that the analysed data comply the assumptions of normality and homoscedasticity (homogeneity of the variance of the groups) thus, two preliminary test must be carried out on the sets of data:

- NORMALLY DISTRIBUTION TESTS: To verify that a particular set of data is normal distributed there are several typologies of tests. The Shapiro-Wilk [17] is one of the most accurate and powerful test for the check of normality, especially for small populations. The null-hypothesis of the test is that the population considered is normally distributed. Thus if the result p-value generated by the test is greater than the significance level chosen (α), the null hypothesis cannot be rejected and the data are considered belong to a normally distribution.

- HOMOSCEDASTICITY TEST: the homogeneity of the variance can be assessed by Levene's test[16]. Such test compares the means and the variances of the populations considered with a significance level chosen. The null hypothesis is that the populations variances are equal and if the p-value resulted from the test is higher than the alpha value chosen, the null hypothesis cannot be rejected.

Once these two requirements are found comply by the populations considered, an ANOVA test can be performed.

Given a number *k* of groups, with n_i samples in the the ith group, can be defined:

$$N = \sum_i n_i = total\ number\ of\ samples\ observed$$

14

$$\bar{x}_i = \frac{1}{n_i} \sum_j x_j = mean\ of\ the\ i^{th}\ group$$

$$\bar{x} = \frac{1}{N} \sum_i \sum_j x_{ij} = overall\ mean\ considering\ all\ the\ results$$

Then the sums of the deviations referred to the differences between the batches, SSB, within the batches , SSW and total, SST are computed:

$$SSB = \sum_i n_i\ (\bar{x}_i - \bar{x})^2$$

$$SSW = \sum_i \sum_j \left(x_{ij} - \bar{x}_i\right)^2$$

$$SST = SSB + SSW$$

The test statistic is the ratio of group and error mean squares divided respectively by their degree of freedom.

$$MSB = \frac{SSB}{k - 1}$$

$$MSW = \frac{SSW}{n - k}$$

$$F = \frac{MSB}{MSW}$$

The statistic F value is then compared to the values of a F-distribution with the same degrees of freedom of the system analysed. If all the previous tests result positive, then it can be assumed that all the data belong to the same population, normally distributed with mean and variance computed with the classical estimator.

2 EXPERIMENTAL ACTIVITY

2.1 MATERIALS AND METHODS

2.1.1 MATERIALS

The materials used in the main industrial processes of Future Fibres are epoxy/carbon prepregs supplied by *Gurit*™. The prepregs used for laminate the various plates under test were all from the series SE84LV/HSC/450, which contain a particular toughened epoxy resin that has excellent compressive properties. This makes them used in large heavily loaded components.

The resin is combined with high strength unidirectional carbon fibres (T700) to form a prepreg system with characteristics reported in Table 2.1 [18] :

Tg	115 °C
Fibres density	1,84 g/cm^3
Matrix density	1,222 g/cm^3
Resin content	35±3%
ILSS	76,24 MPa
Ultimate compression strength σ_{usexp}	1003,27 MPa

Table 2.1: properties of SE84LV/HSC, the prepreg used for the production of all the plates under test.

2.1.2 LAMINATION PROCESSES

Laminates have been produced at Future Fibres headquarters, so the procedures followed were the closest possible to the company standards.

Prepregs rolls were stored at a temperature of -18°C. Before processing, the rolls were required to reach the room temperature. Thus they were extracted from the fridge at least 24 hours before the lamination. Once they were conditioned, the plies were cut from the rolls and, in the case of component with simple geometry such as rectangular plates, this operation was carried out by hand cutter.

Specimens required for ILSS and compressive strength test were machined from plates laminated with 16 plies, all at 0° which respect to the fiber direction. Whereas the material for post impact characterisation was produced with a quasi-isotropic stacking sequence of $[(0/\pm45/90)_s]_s$, for a total again of 16 plies.

2.1.2.1 STANDARD LAMINATION

The plies are carefully stacked on an aluminium plate coated with a PTFE sheet to make the de-moulding operation at the end of the processes easier. After the positioning of the first sheet, debulking is required to obtain a good adhesion between the first ply and the mould.
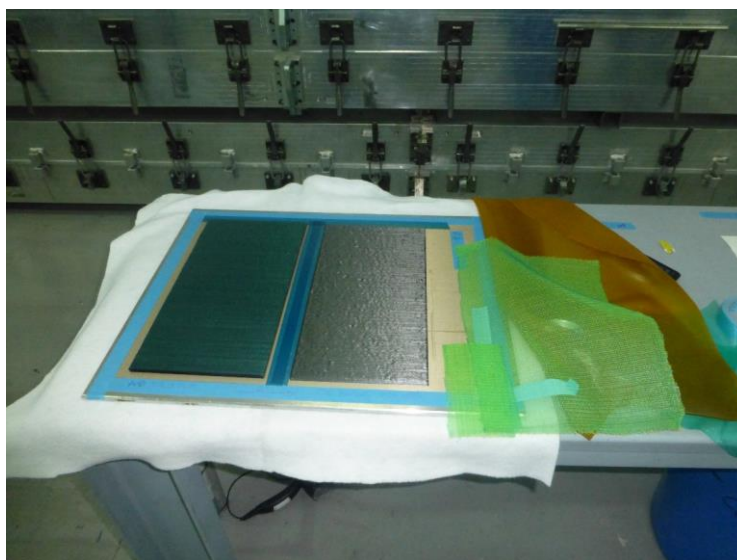
Figure 2.1: Two plates during standard lamination process.

At the top of the stack it was applied a peel ply, then a perforated release film (P3) with holes every 3 cm to help channel the resin extraction during the cure cycle. Over the P3 ply, a breather was then placed to collect the resin squeezed out. At last the laminates were sealed up with a vacuum bag ,ready for the next passage in autoclave.

The followed cure cycle comprehended a dwelling time of 4 hours, at temperature of 75°C. Then the temperature was increased until 93 °C where the crosslinking reaction started and continued for almost 8 hours. The subsequent steps were required to cool down slowly until room temperature the laminates without introducing any thermal shock that could result in rupture or permanent deformation of the components.
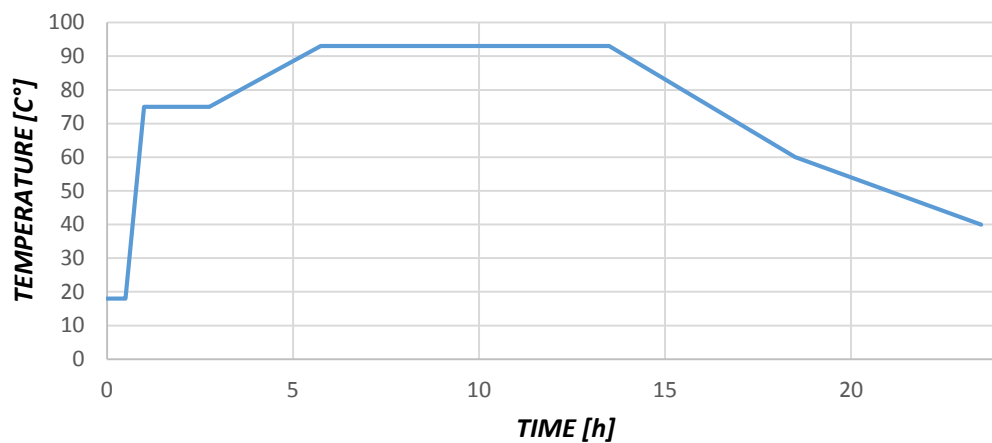
Figure 2.2: Temperature diagram of the standard cure cycle.

A pressure of 5 bar was applied at the start of the dwelling time and kept constant until the end of the crosslink reaction. Then it was progressively reduced at atmospheric level within 4 hours.
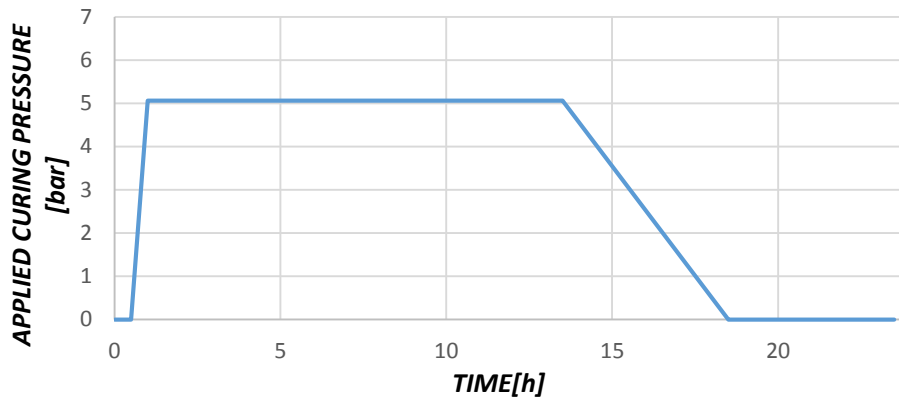
Figure 2.3: Diagram of applied pressure during standard curing cycle

The final plates were then machined in specimens by cutting them with a diamond saw blade. The material so produce are referred as STD series in the next chapters. It has been possible to produce three plates with this procedure (STD_1 STD_2 and STD_3), one for each batch used in the present work, to obtain reference values of the standard process.

2.1.2.2 VARIATION TO STANDARD PROCEDURE

Plates obtained with different processes compared to the STD have been produced in order to study the effects on the mechanical properties.

STD_DB1: during lamination, the operation of debulking has been performed at every plies. This conceptually should correspond in a situation of maximum compaction and density, resulting in a very low voids percentage. Thus, a maximum of mechanical properties were expected from specimens belonging to this plate.

STD_DB0: debulking operation has been performed only after the first ply, just to have a good adhesion with the mould. On the contrary of STD_DB1, an higher percentage of voids was expected.

STD_MIS: STD plates where specimens have been machined with a misalignment ranging from 2° up to 10° which respect to the fibres direction.

STD_QIS: plates that has been laminated following STD process but with a quasi-isotropic lay-up, as required from the standard for drop weight impact test ASTM D7136[19].

NOP_DB1: plates were cured with the same temperature history of STD panels but only in vacuum bag without any pressure applied. In addition, debulking has been performed every layer during lamination.

NOP_DB0: No debulk has been performed during lamination and in addition with a cure cycle without pressure, these plates were expected to have the worst mechanical properties.
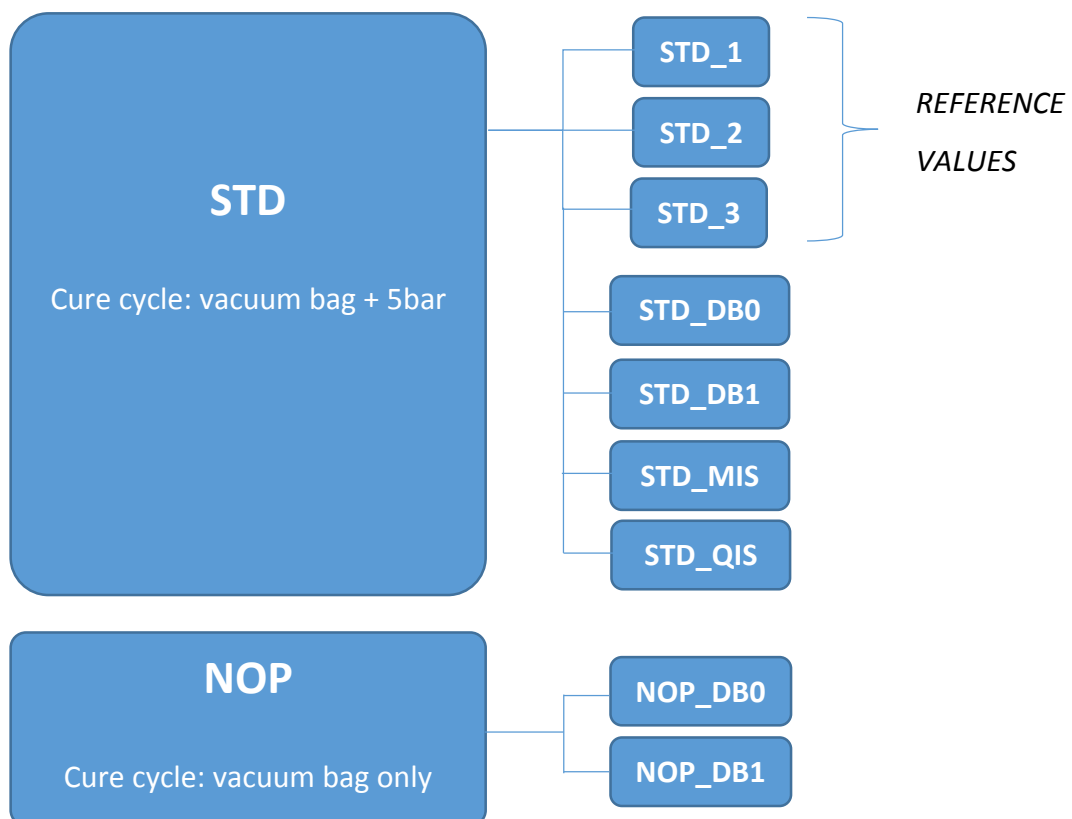
Figure 2.4: Resume of the materials produced.

2.1.3 ULTRASONIC SCANS

Thanks to collaboration with the department of ultrasonic inspection of Alenia-Aermacchi, was possible to scan all the plates with ultrasonic techniques.

Ultrasonic inspection is the most common non-destructive technique used in composite industries and it is useful to detect delaminations, porosity and inclusion that could be generated during the process of laminates. The inspection is divided into two categories: transmission or reflection of ultrasonic signals.

In transmission techniques, an ultrasonic signal is emitted from a probe and passes through the thickness of the specimen. When the signal meets a discontinuity, like a void, it is partially reflected at the interface solid-air whereas the remaining part of the signal is transmitted and collected at the other side of the specimen by a receiver. If the amount of defects found in the path of the sound wave is high, higher will be the attenuation, measured in decibel (dB) (Figure 2.5).
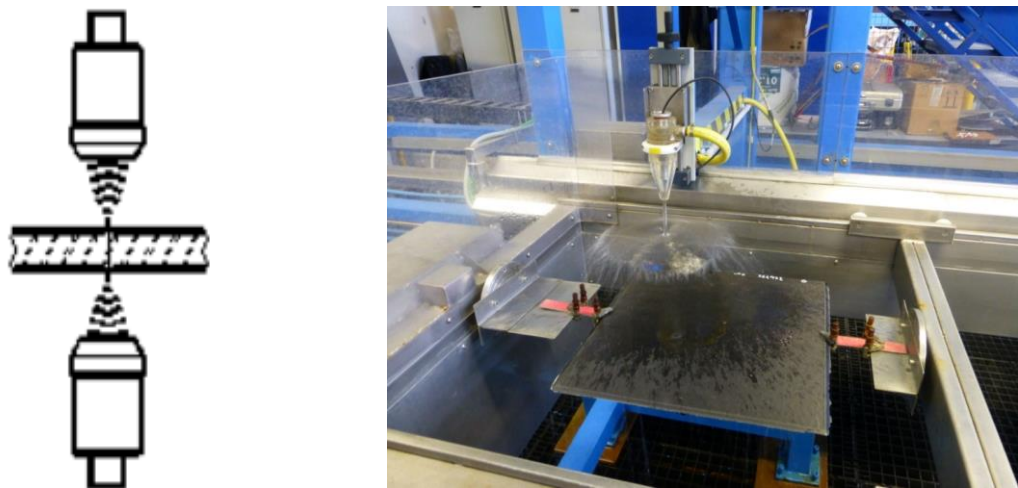
Figure 2.5: Schematization of transmission technique and a practical example on the plates scanned at NDT laboratories of Alenia-Aermacchi.

In reflection, or also called pulse echo, the same probe works both as a transmitter and as a receiver. The probe records a first amplitude peak in the signal when the sound wave reaches the surface of the specimen and a second one due to the back

wall echo (distance E_p in Figure 2.6). Each defect creates other peaks and simultaneously reduces the amplitude of the back wall indication. By analysing the distance between the peaks, it is possible to evaluate the location of the defects along the thickness of the plate.
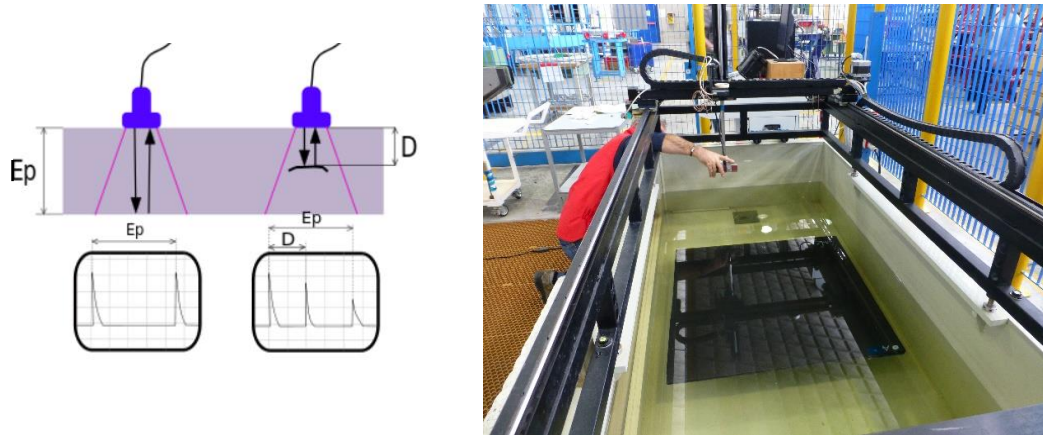
Figure 2.6: Schematization of pulse echo technique and a practical example during the scanner of STD_QIS plate.

All the plates have been scanned in water transmission method to check the effective incidence of the different processes on the quality of the components, except plate STD_QIS, that has been scanned with pulse echo technique due to its dimension. The features of the scanning probes used are listed in the following Table 2.2 and Table 2.3.

PROBE SIGNAL FREQUENCY	5 MHz
GAIN	8,5 dB
PULSER	100 V
SCANNING PASS	1 mm

Table 2.2: Features of the water transmission ultrasonic machine used in the present work.

PROBE SIGNAL FREQUENCY	3,5 MHz
N° OF ELEMENTS OF THE PROBE	128
SCANNING PASS	1 mm

Table 2.3: Features of the pulse echo machine used in for scan STD_QIS machine.

In the following pages will be reported the most significant results obtained at ultrasonic scan.

STD_1	ATTENUATION
MEAN	96,22 dB
STANDARD DEVIATION	0,623 dB

Figure 2.7: Results of ultrasonic scan over STD_1 plate

NOP_DB0	ATTENUATION
MEAN	60,08 dB
STANDARD DEVIATION	5,76 dB

Figure 2.8: Results of ultrasonic scan over NOP_DB0 plate

NOP_DB1	ATTENUATION
MEAN	80,63 dB
STANDARD DEVIATION	4,13 dB

Figure 2.9: Results of ultrasonic scan over NOP_DB1 plate
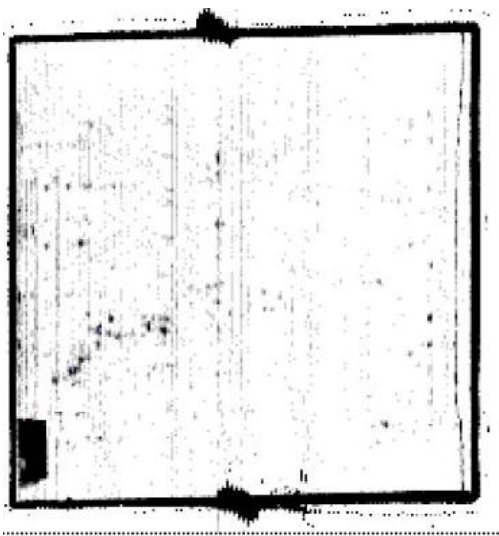
STD_DB0	ATTENUATION
MEAN	96,55 [dB]
STANDARD DEVIATION	0,94 dB

Figure 2.10: Results of ultrasonic scan over STD_DB0 plate
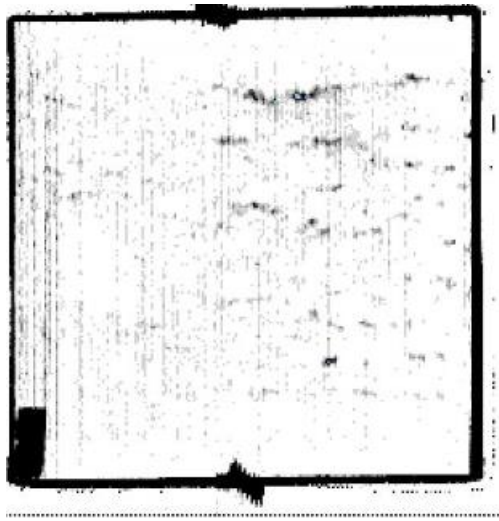
	STD_DB1
MEAN	96,32 dB
STANDARD DEVIATION	0,94 dB

Figure 2.11: Results of ultrasonic scan over STD_DB1 plate

On the basis of the overall results, it has been possible to make the following consideration:

- No defects, such delamination or external inclusion were found in any plates. All the differences in attenuation levels were considered arising from the different level of porosity.

- The reference plates STD had an average attenuation on 96 dB with low standard deviation between $\sigma = 0,623$ dB and $\sigma = 1,26$ dB

- NOP_DB0 and NOP_DB1, as expected, have showed very high attenuations, consistent with the prevision of low compaction. The influence of debulking operation was significant, determining strong difference in the mean attenuations of the two plates: 60 dB for NOP_DB0 and 80 db NOP_DB1. Both the plates has shown also high variability of the signal, $\sigma_{NOP\_DB0} = 5,75$ dB and $\sigma_{NOP\_DB1} = 4,14$ dB, meaning a less homogenous compaction.

- STD_DB0 and STD_DB1 had comparable values with the reference STD plates in both average and dispersion.

2.1.4 VOIDS CONTENT

To have a numerical evaluation of the amount of constituents and voids content, the most common method is to perform an acid digestion. It is a destructive technique which allow to know the volume (or weight) fraction of fibres and matrix, and so, by subtraction, the fraction of voids. The procedure is based on the matrix oxidation with strong acid. The matrix of a specimen is dissolved in concentrated sulphuric acid (96%), provided that the carbon fibres are not attacked. After digestion, the matrix is no longer present in the sample, so the fibres are washed and then weighed. The weight percentage is then calculated:

$$w_f = \left(\frac{M_f}{M_i}\right) * 100$$

<div align="right">23</div>

Where M_f and M_i are respectively the weight of the fibres and the initial weight of the specimen before the acid digestion.

Knowing the density of the fibres, it is possible to obtain its volume fraction

$$\varphi_f = w_f * \frac{\rho_c}{\rho_f}$$

<div align="right">24</div>

With ρ_c the density of the specimen and ρ_f the density of the reinforcement. Similarly, the weight fraction of the matrix and its volume fraction are obtained

$$w_m = \left(\frac{M_i - M_f}{M_i}\right) * 100$$

<div align="right">25</div>

$$\varphi_m = (100 - w_{m)} * \frac{\rho_c}{\rho_m}$$

<div align="right">26</div>

Once known all the previous data, it is possible to compute the voids volume fraction:

$$\varphi_v = 100 - (\varphi_r - \varphi_m)$$

<div align="right">27</div>

The tests have been performed following standard ISO-14127[20] and it may be noted that the procedure presented some issues that may report errors in the evaluation of porosity. First, the porosity had to be uniform and constant in all the plate, no matrix residue had to be found on the fibres after the digestion. In addition, it was required to know the values of density of the matrix, of the fibres and of the plates with a good precision. The values of density for fibres and matrix were supplied by the manufacturer, whereas the values for the final plate has been calculate following the standard ISO-1183.1[21] . Three specimen for each plates of typology NOP and STD_1, STD_2, and STD_3 have been weighted via hydrostatic balance to evaluate the density. The mean values of density, fibres content and voids contents are reported in the following Table 2.4 and for sake of simplicity, rearranged in Figure 2.12 and Figure 2.13.

	ρ_c [g/cm^3]	Std. Dev.	Φ_f	Std. Dev.	Φ_v	Std. Dev.
STD_1	1,5533	0,0046	54,61	0,46	1,31	0,23
STD_2	1,5533	0,0007	55,40	0,62	1,02	0,31
STD_3	1,5444	0,0027	55,63	0,27	0,58	0,14
NOP_DB0	1,5315	0,0064	53,31	1,66	2,18	0,84
NOP_DB1	1,5484	0,0067	54,40	0,32	0,90	0,16
STD_DB0	1,5597	0,0027	56,00	0,82	0,68	0,41
STD_DB1	1,5622	0,0021	55,32	0,35	0,13	0,18

Table 2.4: average density of the plates and mean voids content.
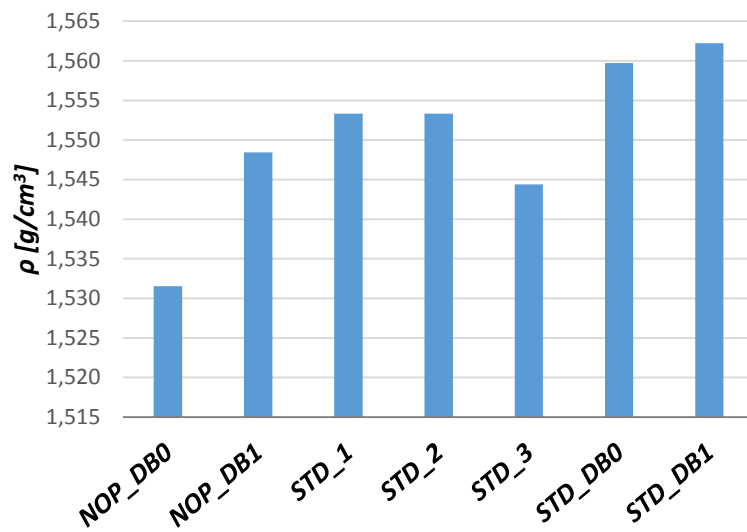
Figure 2.12: Density values measured with the hydrostatic balance

As expected, specimens belonging to the plates cured without pressure have the lowest density values. As it can see from the difference in the mean density from NOP_DB0 and NOP_DB1, debulking plays an important role to the final properties of a component cured only in vacuum bag. The highest value correspond to STD_DB1, where debulking every layer during the lamination result in a higher compaction of the plate once cured. STD_DB0 presents an unexpected high result.
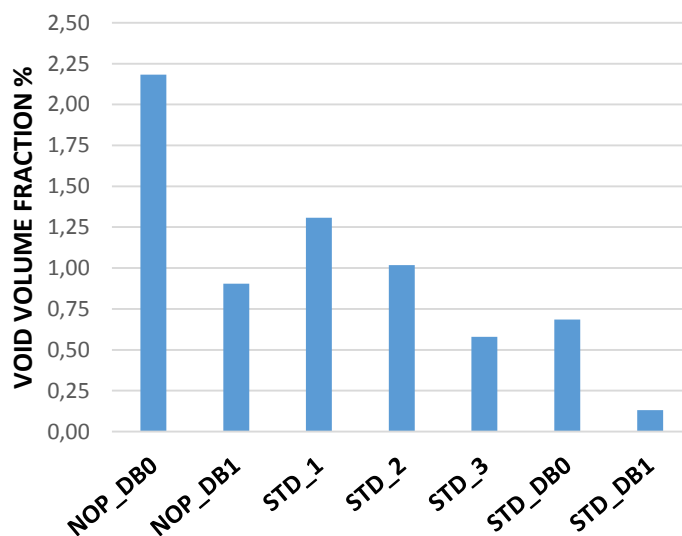
Figure 2.13: Voids contents values calculated by acid digestion.

More dispersion of data was obtained for the voids fraction calculated by acid digestion. In the first attempts of the tests, undissolved matrix was found on the fibres and so longer time than that indicated in the standard was taken for the acid bath to ensure a complete dissolution. In NOP_DB0 and STD_DB1 were found respectively the highest and the lower content of voids, consistent with the prevision. However, for the specimens from the other plates the values obtained were unrelated with the prevision.

2.2 MECHANICAL TESTS

After checked the good quality of the standard reference plates and evaluated the differences in porosity levels for those produced in differents ways, mechanical strength tests were performed.

The tests have been carried out both at the Polymers Engineering Lab and the Department of Structural engineering of Politecnico di Milano. The work has been structured as following. At a preliminary stage, several attempts have been performed to characterise the material strength at a compression test but no one has given reliable result. At ILSS testing, first has been evaluated the strength of samples machined from plates used as references, STD_1 STD_2 and STD_3, to have an indicative value of the standard consolidated process. Second, has been evaluated the impact on strength of the different manufacturing processes represented by the samples from plates STD_DB0, STD_DB1, NOP_DB0 and NOP_DB1. Then, to estimate the impact on strength of a manufacturing defect such as misalignment of plies during lamination, have been carried out tests with samples cut at diverse orientations. Finally, drop-weight tests and subsequently ILSS tests have been performed to understand the influence of impacts, at low velocities and relative low impact energy levels.

2.2.1 COMPRESSION TESTS

Preliminary compression tests were performed at the department of Structural Engineering of Politecnico di Milano. From a plates designed as reference, samples were cut via diamond saw in accordance with the dimensions given by the standard ISO-14126 [22](Table 2.5). The machine at disposition was a MTS machine and the crosshead speed was set at 1mm/min (Figure 2.14).

TYPE OF SPECIMEN	LENGTH [mm]	WIDTH [mm]	THICKNESS [mm]	EXPECTED STRENGTH σ_{USEXP} [MPa]
B2	125	25	7>4	1003,27

Table 2.5: Measure required for the sample of B2 type by ISO ISO14126

Since these were preliminary tests and the interest was on the ultimate compressive strength, no strain gauges were used in this stage. Several attempts were carried out in order to obtain reproducible results but all the samples failed in un-acceptable way. Have been tried different set up for the tests with the purpose to obtain a suitable condition, but no one could gave reliable values.

2.2.1.1 RESULTS

On the first attempt, a group of five specimens were machined and tabbed following the standard [22] indications thus using tabs made by cross-ply glass fibres / epoxy cardboard resin G-10 of 2 mm thickness. The set up was such that the machine applied the load to the specimens by shear loading only through the faces of the end tabs by the clamps.

Figure 2.14: the machine used for the compression tests.

Due to the high loads reached during the test, the specimens slipped in the clamps as it can possible to see in the diagram below ,Figure 2.15, where deviations from linear behaviour are clearly visible. An increase in the pressure of the grips were required to stabilize the samples and Such increase in pressure grips determined a multi-axial state of stress in the tabbed region and a consequent stress concentration that resulted in premature failure.

(a)   (b))
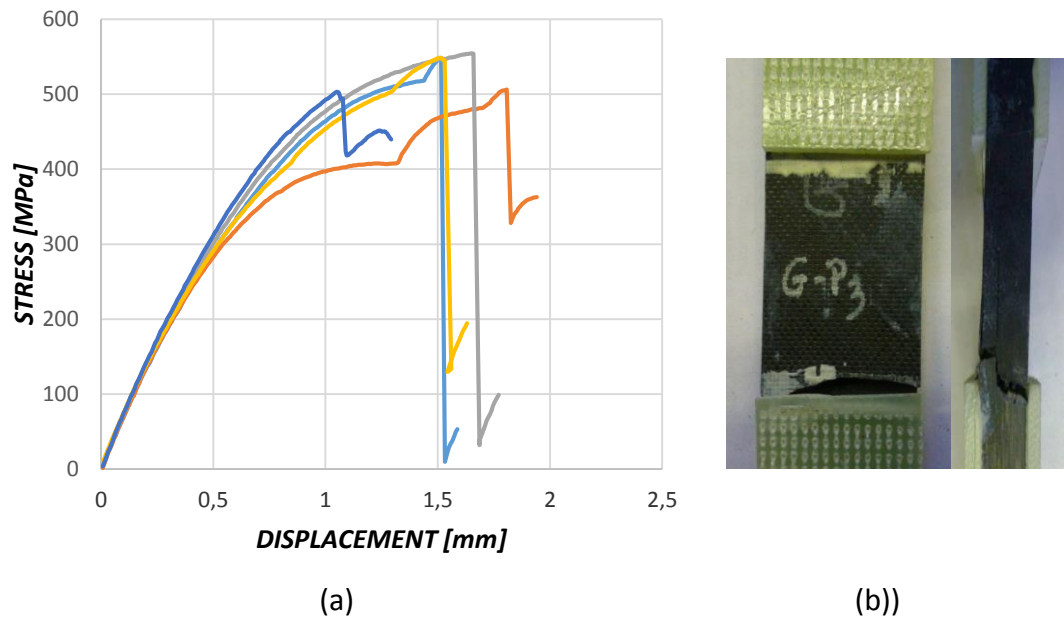
Figure 2.15: (a) Stress-displacement diagram of samples tested at the preliminary testing. (b) Examples of failure obtained.

To avoid this problem different strategies have been attempted:

- Addition of small supports of steel, machined at the department, between the specimens and the crosshead to reduce the pressure at the end tabs. Thus, combining shear loading with end loading, a more homogenous distribution of stresses were expected onto the material (Figure 2.16)

- Reduction of the section of the samples by cutting the specimen along the width. Reducing the cross sectional area, lower loads were needed to bring to rupture the specimens (Figure 2.17).

- Specimens with reduced section were also reduced in length, and tested with a jig as the one specified in the modified ASTM 695[23] (Figure 2.18Figure 2.18).

(a)   (b)
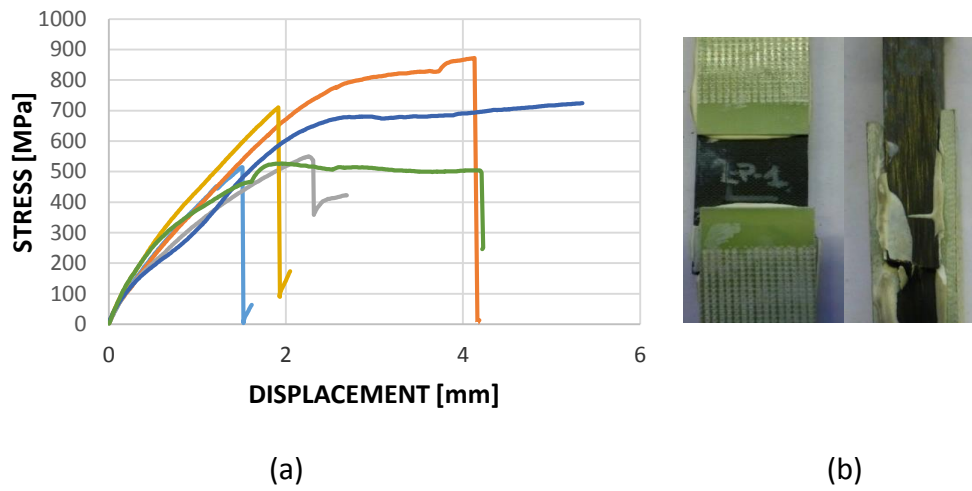
Figure 2.16: (a) Stress-displacement diagram of samples tested with the addition of supports to obtain the combination of shear and end loading (b) examples of failure obtained with the combined set up Shear-end load

(a)   (b)
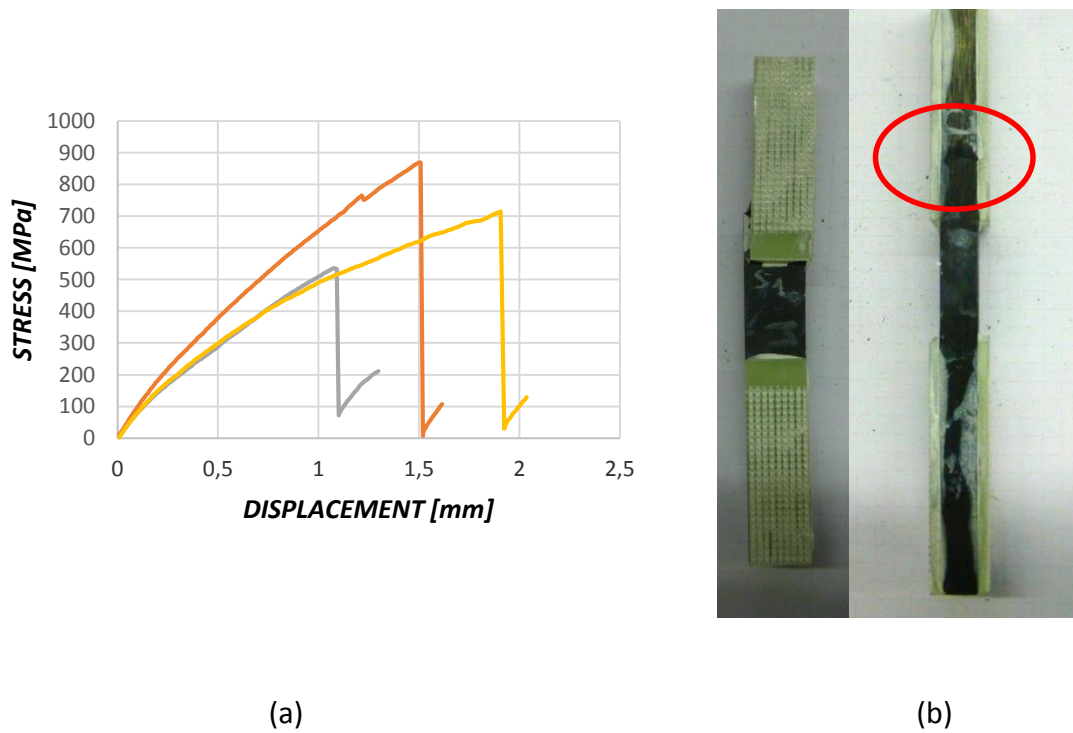
Figure 2.17: (a) Stress-displacement diagram of samples tested with reduced cross-sectional area (b) examples of failure obtained
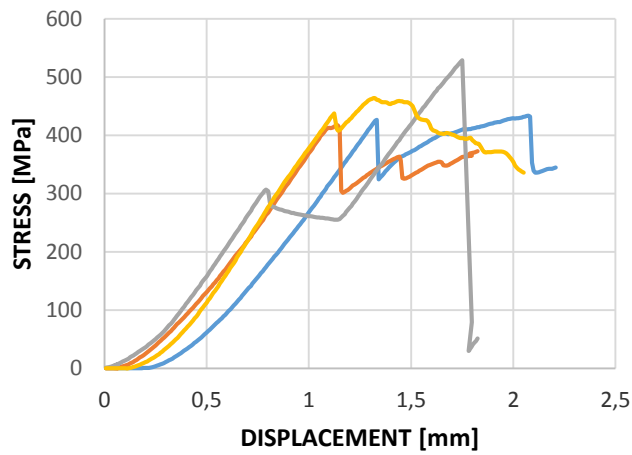
(a)

(b)

Figure 2.18: (a) Stress-displacement diagram of samples tested using the jig as recommended in ASTM D3410 (b) examples of failure obtained

None of the above mentioned strategies were able to give reliable results. In each set up considered, failures occurred always in non-acceptable ways or at load levels excessively low (Table 2.6: Results obtained with the different set up if the machine for compression testsTable 2.6). Since for the STD plate were the samples used have been machined were found of good quality, without defects that could lower of such magnitude the strength, the problems were attributed at the boundary condition of the applying such high loads.

Therefore, it was decided that compressive testing was not possible with the available equipment. The set up tried were not able to give reproducible result with the material at disposition, not even at preliminary testing with the samples produced with the STD procedure. This would have made impossible any type of comparison between different processes.

	MEAN σ_{US} [MPa]	STD. DEVIATION	$\frac{\sigma_{US}}{\sigma_{USEXP}}$ %
ISO COMPRESSION	525,51	34,49	52,38 %
ISO+SMALL SUPPORTS	649,79	142,96	64,77%
ISO+ REDUCED CROSS-SECTIONAL SPECIMEN	706,84	167,05	70,45%
ASTM 695 JIG	649,79	142,96	45,93%

Table 2.6: Results obtained with the different set up if the machine for compression tests

2.2.2 ILSS

ILSS tests have been performed following the guidelines of the standard ISO-14130[9]. The standards provide a method to estimate the apparent interlaminar shear strength based on short beam three-point flexural testing.
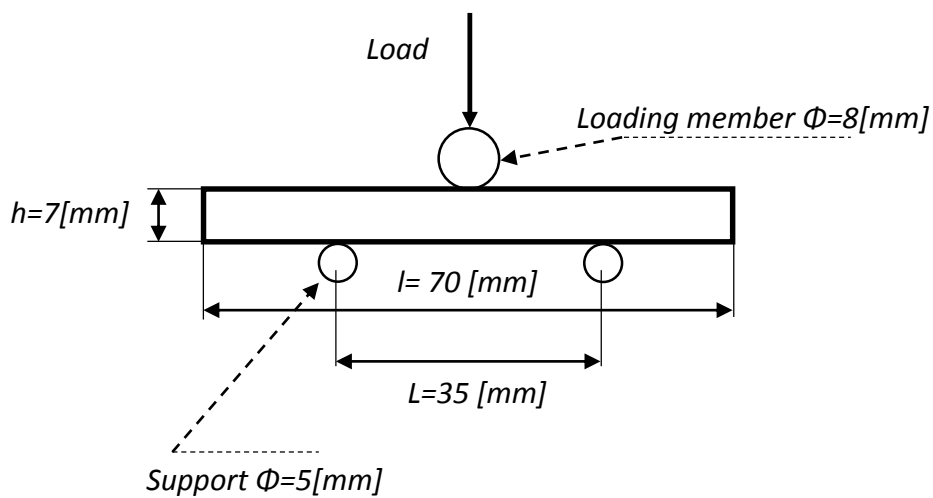
Figure 2.19: Geometry used for the short beam three point flexural testing.

Far from the supports, the shear stress in the sections shows a parabolic trend with maximum value at the neutral axis. In addition, flexural stresses are generated during the test that, on the other hand, are at a maximum on the surface of the specimen and null at the neutral axis. Flexural stresses are known from the short beam theory to being proportional to the span ratio L/h of the specimen and so, minimizing this ratio, the failure tend to occurs when the limit of the interlaminar shear strength is reached.
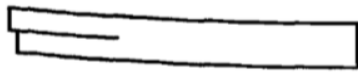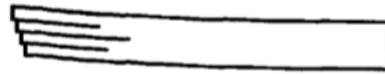
SINGLE SHEAR   *MULTIPLE SHEAR*

ACCEPTABLE FAILURE MODES
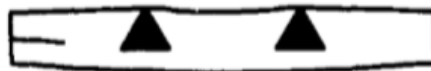
SHEAR AND TENSION   *SHEAR AND*
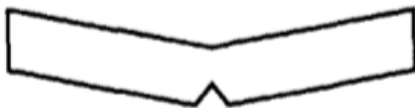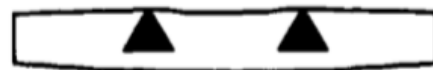
TENSION   *COMPRESSION*

PLASTIC DEFORMATION

NON-ACCEPTABLE FAILURE MODES

Figure 2.20: Acceptable and non-acceptable failure according to ISO14130.

The standard provides a ratio for l/h=10 to ensure a correct failure in the specimen. Even though all the indication of the standard are followed, a complex stress distribution arise on the specimen. The supports and the load zone are critical area that modify the ideal stress distribution predicted by the short beam theory. This may leads to combined typologies of failure, reported in Figure 2.20, and thus a final examination on the rupture is required to discard wrong estimation of the strength. The failure mechanism is ruled by the properties of the matrix and so is strongly affected by the processing that the plates have underwent.

2.2.2.1   RESULTS OF TESTING ON STD PROCESS AND ITS VARIATION

For each plate of different processing typology, a group of 5 specimens were accurately machined via diamond saw and tested. The crosshead displacement velocity of the test machine were set as suggested by the standard to 1mm/min. The setup condition of the test is summarized in the Figure 2.19 whereas the geometry of the specimens are shown in the following Table 2.7. In the next pages will be reported all the results.

	LENGTH l [mm]	STD. DEV.	WIDTH b [mm]	STD. DEV.	THICKNESS h [mm]	STD. DEV.
STD_1	69,91	0,23	24,61	0,09	6,92	0,06
STD_2	70,33	0,08	25,30	0,35	7,13	0,17
STD_3	70,33	0,08	25,30	0,35	7,13	0,17
STD_DB0	70,28	0,03	24,23	0,06	7,29	0,02
STD_DB1	70,44	0,12	25,66	0,10	7,32	0,07
NOP_DB0	70,43	0,10	24,72	0,03	7,63	0,01
NOP_DB1	70,32	0,10	24,88	0,21	7,44	0,13

Table 2.7: Measure of all the specimens tested at this stage of examination.

STD_1

Figure 2.23: Shear stress-displacement diagram result from ILSS tests for STD_1 samples

STD_2

Figure 2.22: Shear stress-displacement diagram result from ILSS tests for STD_2 samples
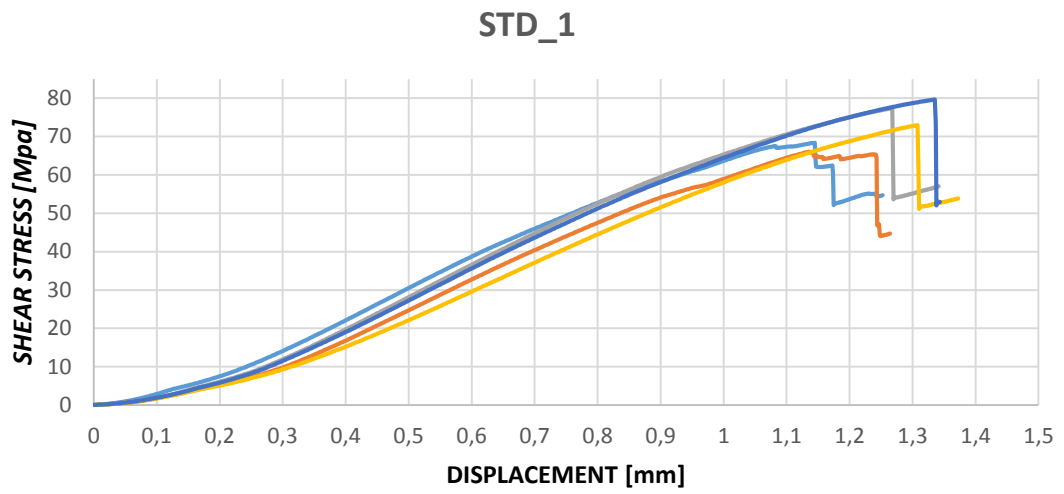

STD_3

Figure 2.21: Shear stress-displacement diagram result from ILSS tests for STD_3 samples

Firstly, results from the standard plates STD_1, STD_2 and STD_3 have been subjected to an ANOVA test to verify the homogeneity of the batches the manufacturing process used. The data have been subjected to the following statistical tests as indicated in chapter 1.6:

	MEAN ILSS[MPa]	STD. DEV.
STD_1	72,90	5,77
STD_2	72,27	3,12
STD_3	76,60	1,47

Table 2.8: ILSS resulting from the tests on the three different batches used as reference.

- TEST ON NORMAL DITRIBUTION

  The results of each group have been subjected to a Shapiro-Wilk test (S.W). The statistic of the test, W, was compared to the reference value W_R taken from S.W. table with significance α=0,05 and the same degree of freedom of the population considered. Then, if the P-value $P(W>W_R)$ was found greater than α, the null-hypothesis of results normally distributed could not be rejected (Table 2.9: Result of the tests to verify the normal distribution of data of the samples from plates STD_1, STD_2, and STD_3.Table 2.9).

- TEST ON HOMOSCEDASTICITY

  A Levene's test has been performed to verify the homogeneity of variances and means of the groups. The statistic F calculated in the test was compared with a reference value $F_R(α,k-1,N-k)$ obtained from the F-test distribution considering a level of significance α=0,05, a number of groups k=3 and the a total number of samples tested N=15. $P(F>F_R)>α$ resulted in the non-reject of the null hypothesis(Table 2.10).

- ANOVA TEST

  Finally, the ANOVA table was calculated. The statistic obtained F was compared to a reference value F_R, with the same feature of the previous test on homoscedasticity (Table 2.10).

	W	$P(W>W_R)$
STD_1	0,9429	0,6862
STD_2	0,9042	0,4333
STD_3	0,8224	0,1218

Table 2.9: Result of the tests to verify the normal distribution of data of the samples from plates STD_1, STD_2, and STD_3.

	F	$P(F>F_R)$
LEVENE'S	3,5425	0,0618
ANOVA	1,8205	0,2039

Table 2.10: Results of the test on homogeneity of variance and its analysis with ANOVA method.

The outcomes of the tests confirmed the homogeneity between the different batches and thus have hallowed to consider the result as belonging to a single population (STD) with mean and standard deviation computed with the classical statistic estimators. This made possible to compare quantitatively the variation in strength between different processes and the reference of the standard. In Table 2.11 are reported all the results in terms of means and standard deviations.

	MEAN ILSS	STD. DEV.
STD	73,93	3,96
STD_DB0	73,91	2,84
STD_DB1	69,94	1,32
NOP_DB0	53,20	1,92
NOP_DB1	65,49	2,86

Table 2.11: All the results of ILSS considering the standard process its variation. The results of the plates STD_1, STD_2, STD_3 considered as a single population with mean and standard deviation calculated with the classical estimator.
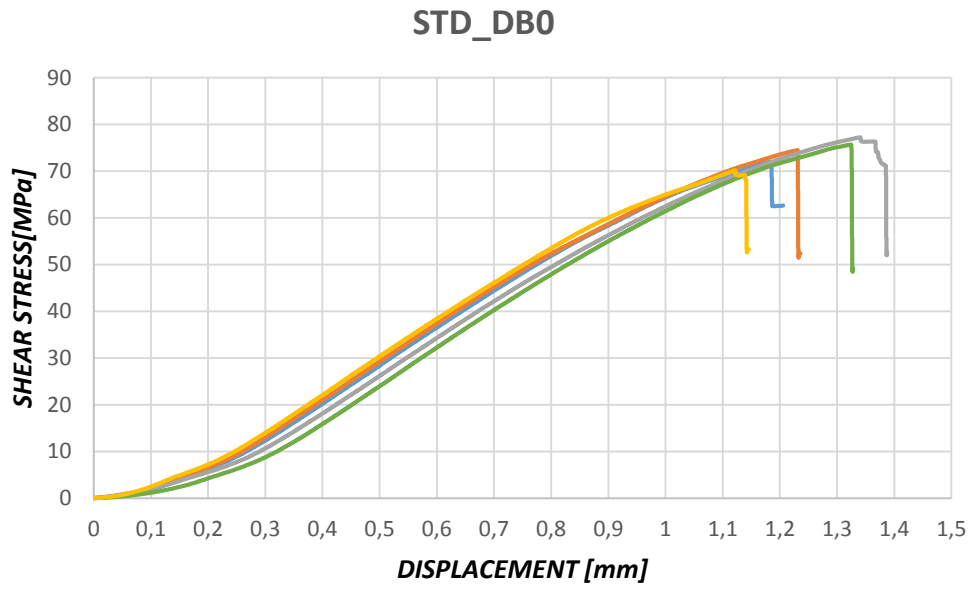
STD_DB0

Figure 2.24: Shear stress-displacement diagram result from ILSS tests for STD_DB0 samples
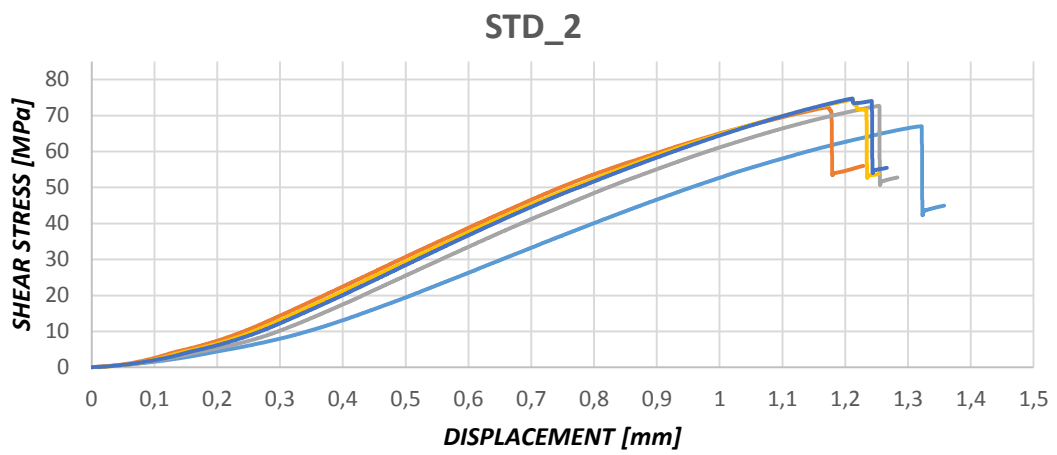
STD_DB1 GROUP
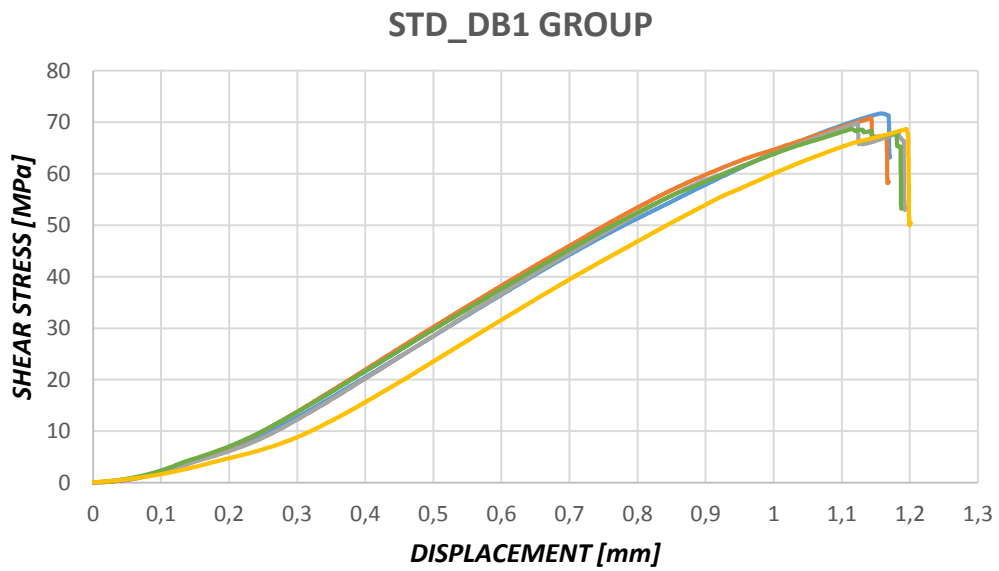
Figure 2.25: Shear stress-displacement diagram result from ILSS tests for STD_DB0 samples

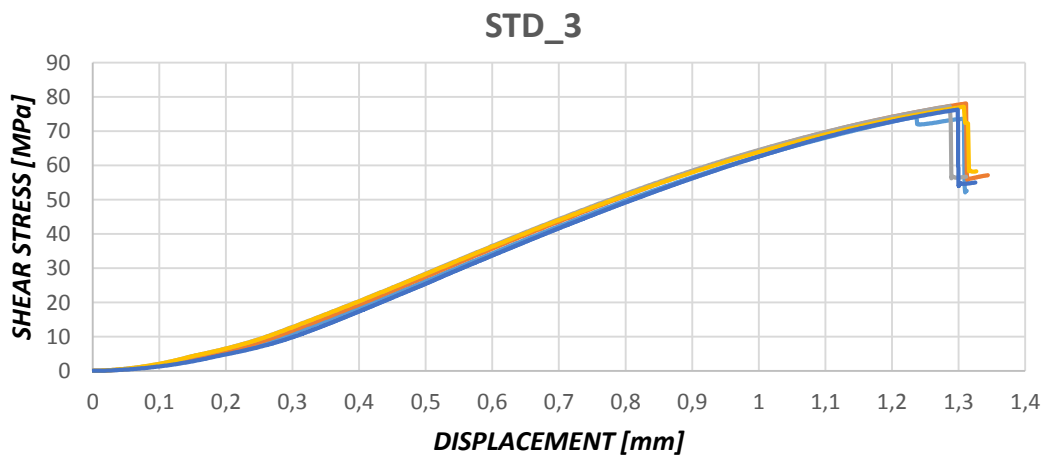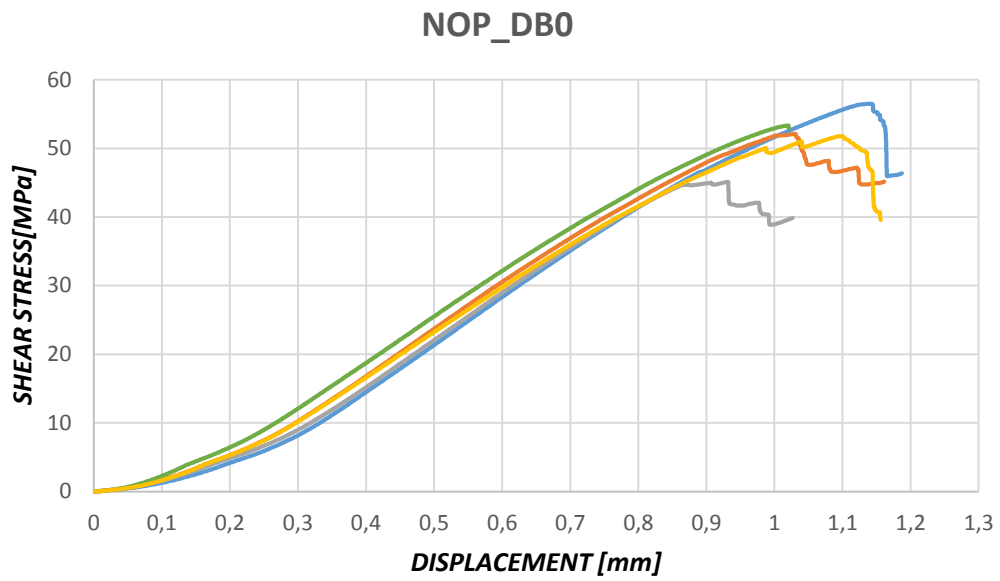*Figure 2.26: Shear stress-displacement diagram result from ILSS tests for NOP_DB0 samples*
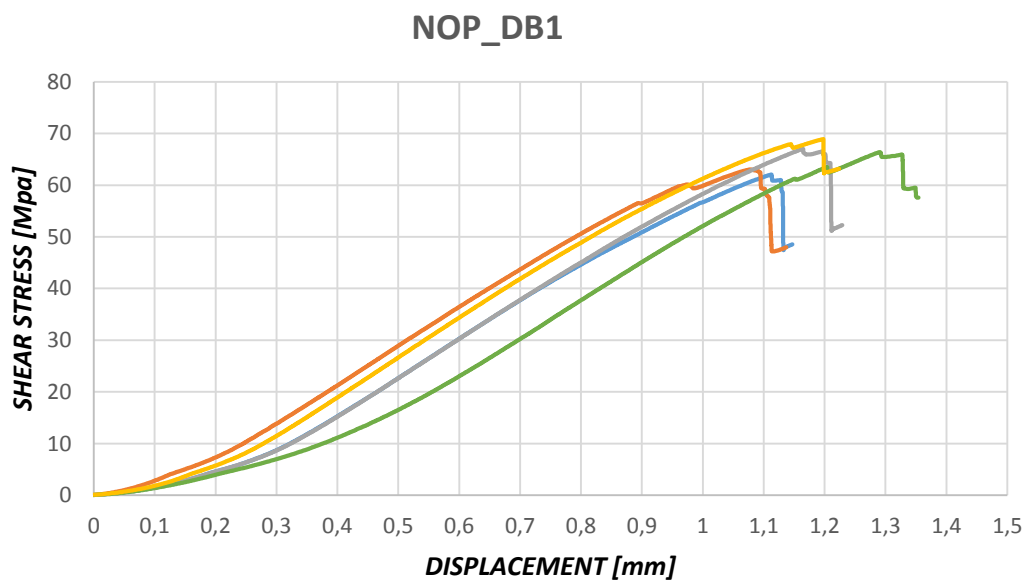
Figure 2.27: Shear stress-displacement diagram result from ILSS tests for NOP_DB1 samples
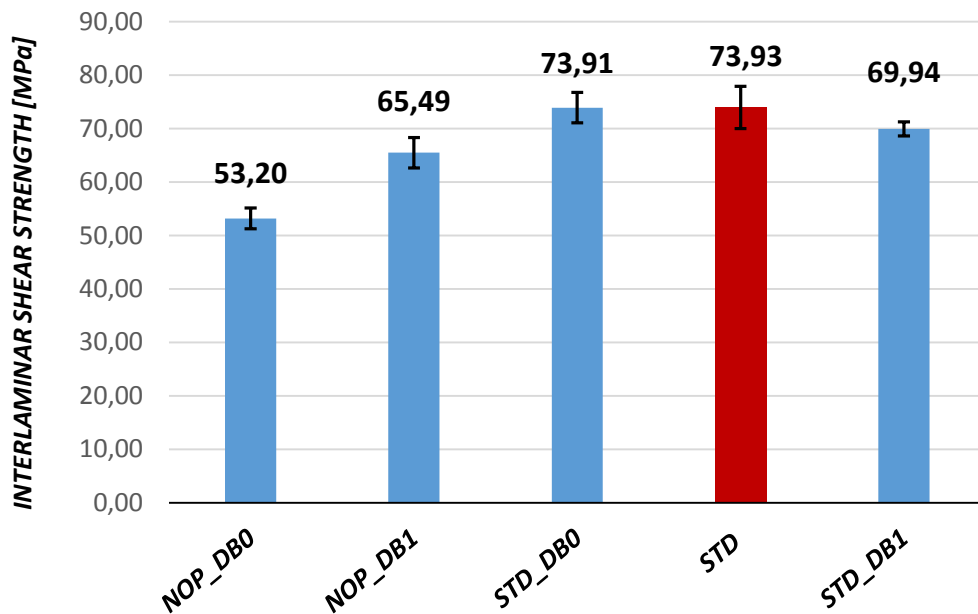
Figure 2.28: Overall results from ILSS for sample of different manufacturing process. Remarked in red the mean of the reference values.

All the specimens belonging to plates cured with the standard curing cycle failed in both single and multiple shear mechanism, accepted by the standard. Specimens belonging to plates of NOP series, on the contrary, failed with no visible cracks on the edges. This typology of failure is not contemplated by the standard ISO 14130 whereas it is for ASTM D2344 [24] (Figure 2.29) and therefore are considered valid in the present work.

Figure 2.29: failure observed in NOP plates as reported in standard ASTM D2344.

Sensible reduction of the mechanical strength has been obtained for NOP plates. NOP_DB0 and NOB_DB1 have shown a decrease of respectively 28% and 11% in strength than the reference values of the standard lamination process. Has been remarked for NOP plates the influence of debulk. Performing every plies or not

performing at all this simple operation, has determined a variation of 17% on the final strength emphasizing the importance to carry out this operation for no-pressure curing cycle. The formation of an excessively high level of porosity is prevented by debulking, that reduce nucleation sites for voids that, without any pressure applied, could easily grow during the curing. The effect of debulk is less marked for plate that underwent STD process. The high pressure itself applied during the consolidation, avoid the formation of nucleation sites and prevent the growth of the already present trapped voids. Samples from STD_DB1, that were expected to have the best mechanical properties, have instead shown comparable result with the sample from the STD reference.

2.2.2.2   RESULT OF TESTING WITH FIBRES MISALINGMENTS
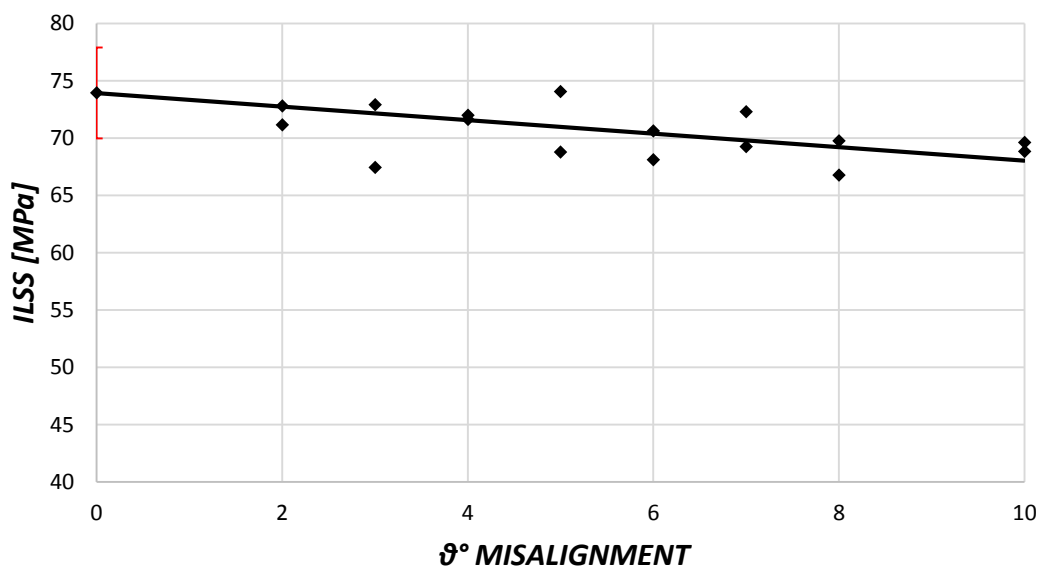
Figure 2.30: Results of tests with various fibres misalignment

Samples with misaligned angles from 2° to 10° degrees were machined from a STD plate STD_MIS, and tested with the purpose to obtain a trend for ILSS at varying the angle Ɵ°. Were also machined and tested samples at a misaligned angle of 15°, but they failed at the supports. In correspondence of high loads, fibres with such a high misalignment tend to stuck on the supports at the edges of the samples and create

regions of stresses concentration. In these regions the stresses arisen are no more only due interlaminar shear, so the failure is not significant in measuring the ILSS. Thus the results for this angles were discarded. On the other hand, the failure obtained for angles ranging from 2° to 10° fell all in the single or multiple shear typology. The results are reported in Figure 2.30: Results of tests with various fibres misalignmentFigure 2.30 and Table 2.12. The points obtained tend to slightly decrease with increasing Ɵ° angle and this trend has been interpolated with a linear regression. The intercept is fixed at the standard reference values ILSS $y_0 = 73,93$ (mean ILSS of STD samples) for Ɵ°=0 and the slope obtained is $m = -0,6383$. The trend observed describe a maximum decrease in ILSS of 9% for a misalignment of $Ɵ° = 10°$.

MISALIGNMENT ANGLES	MEAN ILSS [MPa]	STD. DEV.
2°	71,97	1,16
3°	70,17	3,87
4°	71,82	0,26
5°	72,35	3,74
6°	69,37	1,79
7°	70,77	2,16
8°	68,26	2,10
10°	69,22	0,55

Table 2.12: Result of ILSS testing with sample cut with various misaligned angles

2.2.2.3   RESULTS ON POST IMPACT- ILSS TESTING

Impact tests were carried out at the Polymer Engineering lab at Politecnico di Milano. The purpose was to measure the decrease in strength of samples that have been subjected to impacts at various energy levels. The impact machine at disposition was

a Fractovis 6789 with a hemispheric striker tip of diameter ɸ=20 mm. The striker was able to record the force on the tip during a time of 8ms with a frequency of acquisition of 500 KHz. The samples used have been machined in small panels via diamond saw from a STD plates laminated with quasi isotropic lay up $[(0/\pm45/90)_s]_s$ as indicated in the standard ASTM D7136 [19]. The small panels had dimensions equal to 70 mm in length, 55 mm width and 7 mm in thickness. The layup has been defined such that the 0° fiber orientation is aligned with the lengthwise dimension. Then, specimen were impacted at the centre with energy ranging from 0,5 to 34,85J. Once impacted, the edges have been machined and reduce in width to up to 25 mm to be subsequently tested in interlaminar strength with the three point flexural short beam test.

A group of five samples have not been impacted and have been tested only in ILSS test. The mean of the results of this group, reported in Table 2.14, has been set as a reference for the strength, in order to be compared with the impacted ones. All the reference specimens tested have shown a multiple shear failure mechanism (Figure 2.20).

	LENGTH l [mm]	STD. DEV.	WIDTH b [mm]	STD. DEV.	THICKNESS h [mm]	STD. DEV.
STD_QIS	70,65	0,67	25,50	0,81	6,98	0,08

Table 2.13: Dimensions of all the samples STD_QIS subjected to ILSS testing

	MEAN ILSS [MPa]	STD DEV.
STD_QIS (*non-impacted*)	40,19	2,80

Table 2.14: Result of ILSS test for non-impacted STD_QIS samples.

2.2.2.4 IMPACTED SAMPLES

Various impact energy have been obtained by changing the weight on the striker or the height of the drop test, depending on the level of energy required. For low impact energy, a weight of 3,153 kg has been used whereas, in order to not exceed the height of the machine, weight ranging from 6,153 to 11,153 kg have been used for medium and high impact energy level. Up to 5,4J panels have been impacted with increasing energy of about 0,5J each step. Then, as energy was increasing, much higher steps were adopted, starting from 1J up to 3J for very high energy. Repeated tests has been performend at low impact energies to well understand the behaviuour. On the contrary, at high energies the behaviour was already clear without the necessity to repeat tests.

Velocity of impact ranging from 0,56 up to 2,5 m/s has been used, thus ensuring that the low velocity impact hypothesis was respected.

Figure 2.31: The Fractovis 6789, the machine used to impact the samples.

At a first visual inspection on the surface of the impacted regions, for samples that underwent impact up to 4,83J were almost impossible to localize the zones hit by the striker. No effects on the surface were detected. On the other hand, for impact energy above 15J, signs of the hit were visible only on the side of the impact in form of light indentation though did not exhibit cracks. On the samples impacted with energy from 5,40 up to 15,66J the damage was considered to fall in the barely visible classification. The results of the inspection are summed up in the below Table 2.15 :
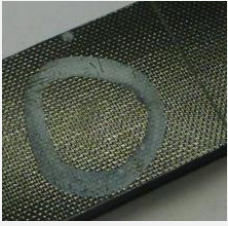
IMPACT ENERGY [J]	VISUAL INSPECTION	
0,5 ÷ 4,83	NON VISIBLE	
5,40 – 15,66	BARELY VISIBLE	
18,31 – 34,85	VISIBLE	

Table 2.15: Results of visual inspection on impacted samples

Analysing the force-time diagrams recorded by the striker it is possible to draw some consideration.
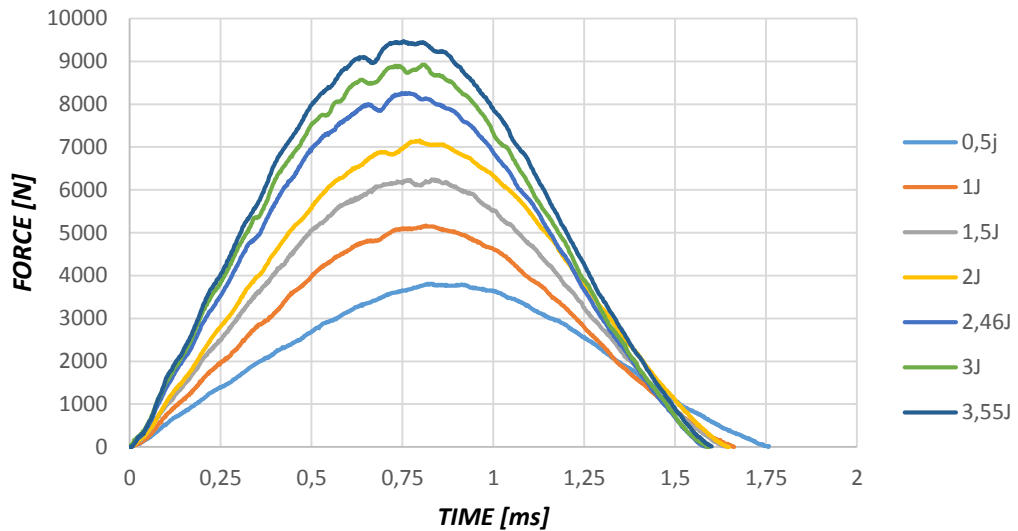
Figure 2.32: Force-Time diagrams obtained at low impact energy, ranging from 0,5J up to 3,55J

For impact energy up to 3,55J the diagram obtained are reported in Figure 2.32. It is possible to observe smooth curves and almost sinusoidal, with little oscillations due to natural frequencies of the panels which reach a maximum increasingly higher with increase energy. It is possible to set this value as a threshold, called E_{t1} and observe that for higher impact energy, the diagram show an important force signal fall followed by oscillations resonance (Figure 2.34 and Figure 2.33), characteristic of damage onset. With increasing energy, the peak force does not increase more since it is the value where the first failure take place in the material. However, increases the maximum force registered which is related to oscillation modes of the material and not to the failure mechanism happening on each plies.

Figure 2.33: Force-Time diagrams obtained at low impact energy, ranging from 4J up to 34,85J
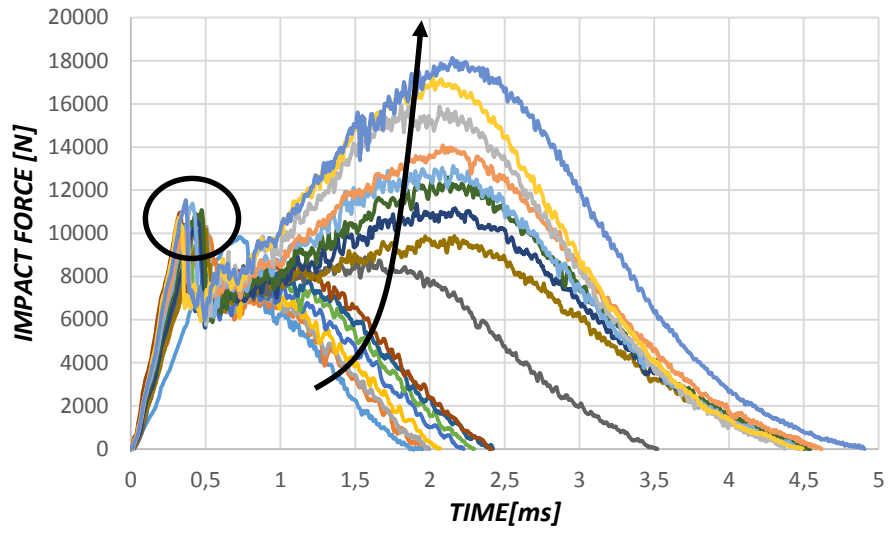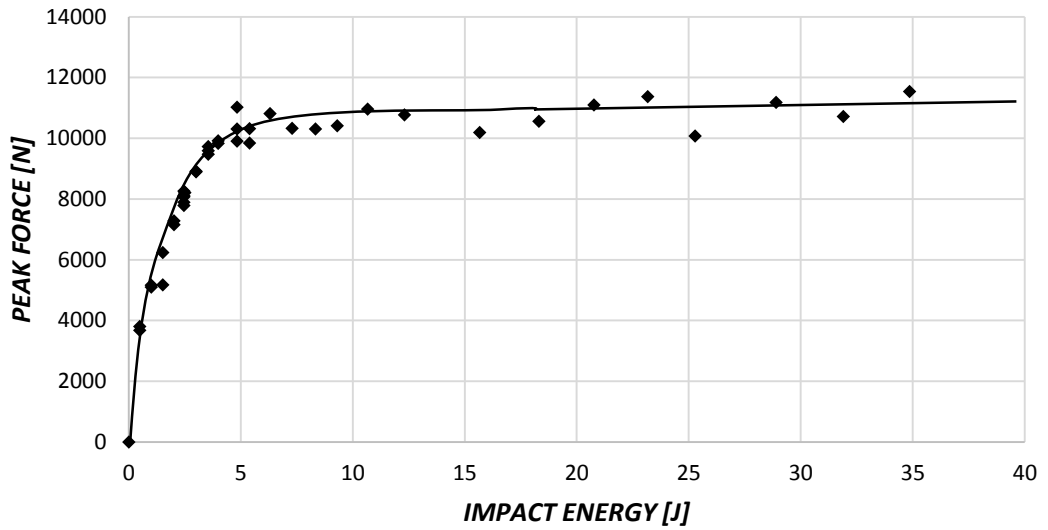

Figure 2.34: Peaks force against impact energy. Clearly visible the plateau above the threshold energy.

The results obtained at the ILSS test confirmed the previous consideration on
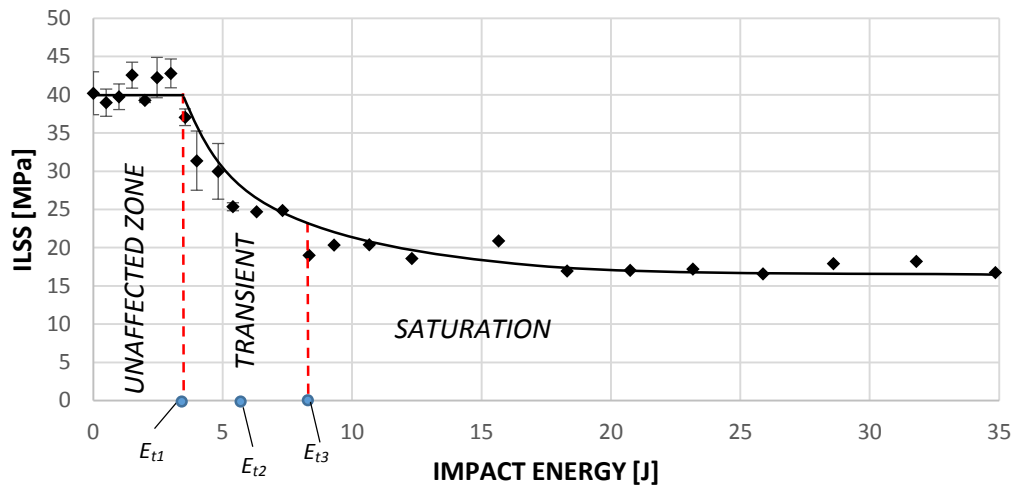
Figure 2.35: Interlaminar shear strength against various impact energy

The interlaminar strength were not affected by impact until E_{t1} was not exceeded. In this range, the samples were found behave as the non-impacted ones. Above the threshold, the strength rapidly decrease. It has been observed that for energy slightly higher than E_{t1}, until samples tested at 4,83J (E_{t2}), the specimens still failed by a sudden rupture. In the range E_{t1}- E_{t2}, delaminations were always found start where transverse matrix cracks due to impact were present, as they offer suitable stress concentration zones where delamination could nucleate and propagate.
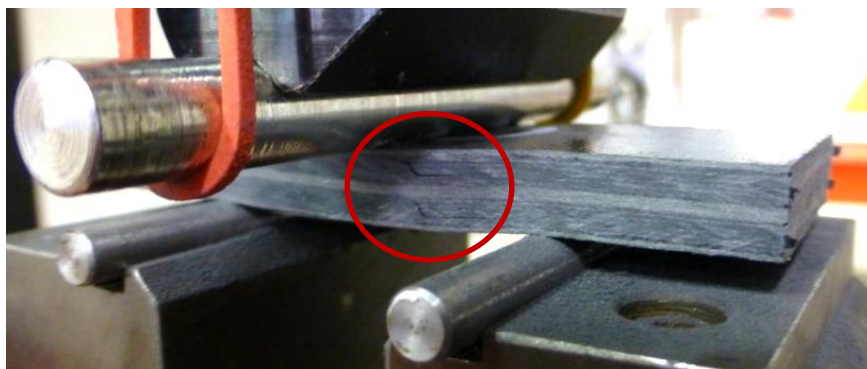
Figure 2.36: Failure found in samples impacted with energy up to 4,83J, tested in ILSS

For higher impact energy, above E_{t2}, samples didn't show a sudden rupture but a progressive reduce in stiffness until the sample were still able to deform but no more load was bear(Figure 2.37). It was visible the formation of a growing number of small matrix cracks and the progressive opening of voids between plies. The explanation is

that above E_{t2} the impact energy was able to determine also the onset of delaminations and thus, at a subsequent short beam test the samples resulted as already failed by this mechanism. For these impact energy levels, the property measured on the short beam test were no more the ILSS but rather the maximum shear stress bearable. With increasing impact energy a strong reduction in stiffness was observed, as delaminations were affecting more interfaces, but the maximum stress borne didn't change with the same magnitude (Figure 2.35, Figure 2.37).By focusing on the residual strength and analysing the results reported in Figure 2.35 three regions are finally identifiable.
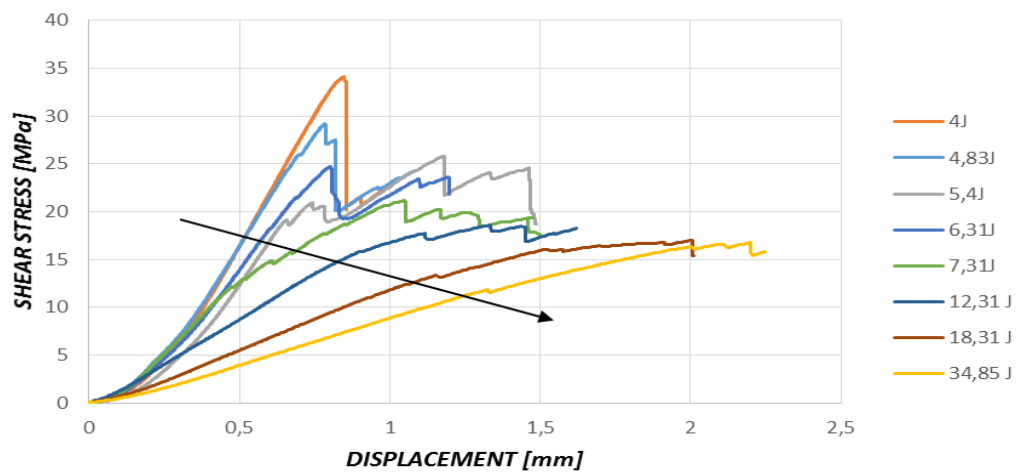
Figure 2.37: Shear stress against displacement for samples impacted above Et1 in the range 4J-34,85J. For sake of semplicity not all the samples are reported.

1. UNAFFECTED ZONE: with impact energy up to E_{t1}, the ILSS is not affected at all by the drop-weight tests.

2. TRANSIENT: with energy above E_{t1} up to 8,34J, called it E_{t3}, is possible to observe a transient where ILSS/maximum shear stress bearable decrease of about 47%

3. SATURATION: After the transient, above E_{t3}, the maximum shear stress registered varied only of 6% passing from 47% of the reference value to 41% .

IMPACT ENERGY [J]	EFFECT ON STRENGTH	MEAN ILSS [MPa]	STD. DEV.	TYPE OF DAMAGE	RESIDULAL ILSS %
0	UNAFFECTED ZONE	40,19	2,80	*NON VISIBLE*	100,00
0,5	|	38,97	1,77	|	96,97
1	|	39,76	1,67	|	98,92
1,5	|	42,58	1,70	|	105,94
2	|	39,28	0,29	|	97,73
2,46	|	42,25	2,64	|	105,12
3	|	42,80	1,89	|	106,49
3,55	⊥	37,05	1,09	|	92,19
4	*TRANSIENT ZONE*	31,38	3,88	|	78,07
4,83	|	29,97	3,64	⊥	74,56
5,4	|	25,37	0,53	*BARELY VISIBLE*	63,12
6,31	|	24,73	-------	|	61,52
7,31	⊥	24,87	-------	|	61,88
8,34	*SATURATION ZONE*	19,01	-------	|	47,30
9,31	|	20,36	-------	|	50,65
10,66	|	20,41	-------	|	50,78
12,31	|	18,61	-------	|	46,31
15,66	|	20,89	-------	⊥	51,98
18,31	|	16,98	-------	*VISIBLE*	42,24
20,74	|	17,04	-------	|	42,39
23,17	|	17,21	-------	|	42,81
25,88	|	16,57	-------	|	41,23
28,6	|	17,90	-------	|	44,55
31,8	|	18,22	-------	|	45,33
34,85	|	16,76	-------	|	41,71

Table 2.16: Results of impact and post-impact characterisation divided by the effects of impact energy on strength.

3 CONCLUSIONS

The work here presented has taken into account the influence on strength of both different laminations processes and defects that may occur during manufacturing of carbon fibres reinforced composite with thermoset matrix, commonly used in the marine sector.

Ultrasonic scan, which is a widely used NDT employed in composite manufacture, has been helpful to remark different compaction levels between the panels produced. The variation of the frequency at which operation of debulk was performed during the lamination, has turned out to determine strong variation in porosity levels in the plates cured without pressure (NOP_DB0 and NOP_DB1). Whereas for plates cured with pressure (STD series) it was not noticed any significant change.

To have an effective measure of the voids contents, density and acid digestion tests have been performed. The results have confirmed the consideration based on ultrasonic analysis for NOP_DB0 and NOP_DB1 whereas an unexpected high value in density has been obtained for STD_DB0. The measure of void content by acid digestion has instead revealed scatter in the results.

The strength of the materials has been proved trough subsequent mechanical tests. Different set up has been tried in order to obtain reproducible and comparable data from compressive test but no one could give reliable results. The high loads required to bring at rupture the specimens, created instability in the machine used and resulted in premature failure.

At ILSS tests has been observed homogeneity of result on testing different batches produced following the standard procedure. It has been verified a significant decrease in strength up to 28% (NOP_DB0) and a significant variation of 17% in strength between plates NOP_DB0 and NOP_DB1 giving a numerical evaluation of the importance of the debulk operation in cure cycle without pressure. No significant variation in strength has been obtained in the STD series plates produced .

The same characterisation has been carried out with samples from a STD plate and different fibres misalignment , ranging from 0° up to 10° denoting a linear decrease in ILSS strength up to 9% for the samples machined with a misalignment of 10°.

From a plate laminated with STD process and a quasi-isotropic lay-up, small panels has been machined and tested at drop-weight impact tests and then measured the decrease in ILSS. An important influence has been observed already at low impact energy level. It has been found that when the damage of the impact became classifiable as barely visible (above 5,4J), the material has already delaminated and the maximum shear that can bear is only at 63% of the value of the non-impacted ones.

REFERENCES

1. Garret, R., *The Symmetry of Sailing - The Physics of Sailing for Yachtsmen.* 1987(3): p. 39-42.

2. Marsh, G. and A. Jacob, *Trends in marine composites.* Reinforced Plastics, 2007. **51**(2): p. 22-27.

3. P. Nogueira, C.R., A. Torres, M. J. Abad, J. Cano, J. Lopez, I. Lopez-Bueno, L. Barral, *Effect of water Sorption on the Structure and mechanical properties of an Epoxy Resin System.* Journal of applied polymer science, 2001. **80**(1).

4. Mallick, P.K., *FIBER-REINFORCED COMPOSITES: Materials, Manufacturing, and Design.* 2008(4.1.5).

5. Donnet J.B., R.S., Wang T.K., Peng C.M., *Carbon Fibres.* 1998: p. 3-30.

6. Barbero, E.J., *Introduction to composite materials design.* 1999: p. 48-49.

7. Fleck, N.A., *Compressive Failure of Fiber Composite.* Advances in Applied Mechanics, 1997. **33**: p. 43-85.

8. S.H. Lee, A.M.W., *Compressive response and failure of fiber reinforced unidirectional composites.* International Journal of Fracture, 1999.

9. STANDARD, I., *ISO-14130: Fibre-reinforced plastic composites - Determination of apparent interlaminar shear strength by short-beam method*

10. l. Liu, B.M.Z., D.F. Wang, Z.J. Wu, *Effects of cure cycles on void content and mechanical properties of composite laminates.* Composite Structures, 2005.

11. Hernández, S., et al., *Effect of curing cycle on void distribution and interlaminar shear strength in polymer-matrix composites.* Composites Science and Technology, 2011. **71**(10): p. 1331-1341.

12. Allen J. Fawcett, G.D.O., *Boeing Composite Airframe Damage Tolerance and Service Experience.* Boeing Commercial Airplanes, 787 program.

13. C. Soutis, P.T.C., *Prediction of the post-impact compressive strength of CFRP laminated composite. .* Composites Science and Technology 1996.

14. G.A.O. Davies, D.H., J. Wang, *Prediction of threshold impact energy for onset of delamination in quasi-isotropic carbon/epoxy composite laminates under low-velocity impact.* Composite science and technology, 2000.

15. M.0.W. Richardson, M.J.W., *Review of low-velocity impact properties of composite materials* 1996.

16. Departmen of defense, U.s.o.A., *Composite Materials Handbook.* 2002. **1**(8): p. 28-32.

17. S.S. Shapiro, M.B.W., *An Analysis of Variance Test for Normality.* Biometrika, 1965. **52**: p. 591-611.

18. Gurit, *SE84LV Datasheets.*

19. INTERNATIONAL, A., *ASTM D7136 - Standard Test Method for Measuring the Damage Resistance of a Fiber-Reinforced Polymer Matrix Composite to a Drop-Weight Impact Event.*

20. STANDARD, I., *ISO-14127: Carbon-fibre-reinforced composites-Determination of the resin, fibre and void contents.*

21. STANDARD, I., *ISO-1183-1: Plastics — Methods for determining the density of non cellular plastics.*

22. STANDARD, I., *ISO-14126: Fibre-reinforced plastic composites - Determination of compressive properties in the in-plane direction.*

23. INTERNATIONAL, A., *ASTM D695: Standard test method for compressive properties of rigid plastics.* 1996.

24. INTERNATIONAL, A., *ASTM D2344/D2344M Standard Test Method for Short-Beam Strength of Polymer Matrix Composite Materials and Their Laminates.*